Analysis of Washout Filter-Based Power Sharing Strategy - An Equivalent Secondary Controller for Islanded Microgrid without LBC Lines

Han, Yang; Li, Hong; Xu, Lin; Zhao, Xin; Guerrero, Josep M.

Published in:
I E E E Transactions on Smart Grid

DOI (link to publication from Publisher):
10.1109/TSG.2017.2647958

Publication date:
2018

Analysis of Washout Filter-Based Power Sharing Strategy—An Equivalent Secondary Controller for Islanded Microgrid without LBC Lines

Yang Han, *Member*, *IEEE*, Hong Li, Lin Xu, Xin Zhao and Josep M. Guerrero, *Fellow*, *IEEE*.

***Abstract*—As a supplement of the droop control, the concept of secondary controlled microgrid (MG) has been extensively studied for voltage and frequency restoration. However, the low band-width communication (LBC) channels are needed to exchange information between the primary and secondary controllers, and the performance of the secondary controller degrades due to the uncertain communication delay and data drop-out in the LBC lines. Recently, a washout filter-based power sharing method was presented without communication lines and additional control loops. In this paper, the equivalence between secondary control and washout filter-based power sharing strategy for islanded microgrid is demonstrated, and the generalized washout filter control scheme has been obtained. Additionally, the physical meaning of control parameters of secondary controllers is also presented. Besides, a complete small-signal model of the generalized washout filter-based control method for islanded MG system is built, which can be utilized to design the control parameters and analyze the stability of MG system. Finally, extensive simulation and experimental results are provided to confirm the validity and effectiveness of the derived equivalent control scheme for islanded MG.**

***Index Terms*—microgrid, droop control, washout filter, communication delay, small-signal model, secondary control, band-pass filter (BPF), hardware-in-the-loop (HIL).**

Manuscript received February 07, 2016; revised August 02, 2016, and November 22, 2016; accepted December 30, 2016. This work was supported in part by the National Natural Science Foundation of China under Grant No. 51307015, and in part by the State Key Laboratory of Power Transmission Equipment & System Security and New Technology under Grant No. 2007DA10512713405, and in part by the Open Research Subject of Sichuan Province Key Laboratory of Power Electronics Energy-Saving Technologies & Equipment under Grant No. szjj2015-067, and in part by the Open Research Subject of Artificial Intelligence Key Laboratory of Sichuan Province under Grant No. 2015RZJ02, and in part by the Fundamental Research Funds of Central Universities of China under Grant No. ZYGX2015J087. Paper no. TSG-00183-2016.

Y. Han and H. Li are with the Department of Power Electronics, School of Mechatronics Engineering, University of Electronic Science and Technology of China, No.2006, Xiyuan Avenue, West Hi-Tech Zone, Chengdu 611731, China (e-mail: hanyang@uestc.edu.cn; Li_Hong01@126.com).

L. Xu is with the Sichuan Electric Power Research Institute, Sichuan Electric Power Company, Chengdu 610072, China (xulinn@163.com).

X. Zhao and J. M. Guerrero are with Department of Energy Technology, Aalborg University, 9220 Aalborg, Denmark (e-mail: {xzh, joz}@et.aau.dk).

Color versions of one or more of the figures in this paper are available online at http://ieeexplore.ieee.org.

Digital Object Identifier ******/TSG.*******

NOMENCLATURE

Abbreviations

MG	Microgrid.
LBC	Low band-width communication.
BPF	Band-pass filter.
HIL	Hardware-in-the-loop.
DG	Distributed generation.
RES	Renewable energy resource.
PCC	Point of common coupling.
MAS	Multi-agent system.
PI	Proportional integral.
PR	Proportional resonant.
LPF	Low-pass filter.
SW	Switch.

Variables

i_{ld}, i_{lq}	Inverter currents in *dq*-axis.
i_{od}, i_{oq}	Output currents in *dq*-axis.
i_{line}	Line currents in *dq*-axis.
i_{load}	Load currents in *dq*-axis.
v_{od}, v_{oq}	Actual output voltages of inverters in *dq*-axis.
p, q	Instantaneous active and reactive powers.
P, Q	Measured averaged active and reactive powers through a low-pass filter.
v_d, v_q	Output voltages of power controllers in *dq*-axis.
Δ	Small deviation of the state variable.

Parameters

ω_c	Cut-off frequency of the LPF.
ω^*, v^*	Rated angular frequency and voltage amplitude in droop controllers.
ω^*_{MG}, v^*_{MG}	Rated angular frequency and voltage amplitude in secondary controllers.
ω, v	Angular frequency and voltage amplitude of the islanded microgrid.
ω_{sec}, v_{sec}	Compensation of the angular frequency and voltage amplitude from secondary controllers.
$k_{p\omega}$, $k_{i\omega}$	Parameters of the frequency restoration control.
k_{pE}, k_{iE}	Parameters of the voltage restoration control.
m_p, n_q	Frequency and voltage droop coefficients.
k_p, k_q	Parameters of washout filter-based controller.
ω_0	Fundamental frequency.
L_{line}, r_{line}	DG feeder inductance and resistance.
L_f, r_{Lf} L_c, r_{Lc}	Filters inductance and resistance.

L_{load}, r_{load}	Load inductance and resistance.
C_f	Filter capacitance.
τ	Response time.
τ_d	LBC delay.
r_N	Virtual resistance.
k_{pv}, k_{iv}	Parameters of the voltage controller.
k_{pc}, k_{ic}	Parameters of the current controller.

I. Introduction

DISTRIBUTED generation (DG) using renewable energy resource (RES), including fuel cells, solar power plants and wind turbines, is attracting more and more attention for its capability to meet the increased demand for electricity to reduce pollution, decrease power transmission losses and improve the local utilization of RESs [1-3]. However, the voltage deviations, inverse power flow, and voltage fluctuations caused by the high penetration level of the DG systems are causing serious power quality problems, which affects the stable operation of the electric power systems [4-6]. To solve these problems and coordinate different types of DG units effectively using local power management systems, the concept of the microgrid (MG) as a promising approach has been widely accepted [7-9].

Compared to the conventional distributed power generation systems, a microgrid has enhanced control flexibilities to fulfill system reliability and power quality requirements, which can operate in either grid-connected or islanded mode [3-7]. When MG operates in the case of grid-connected mode, where the upstream grid participates in supplying the demand of the load, it should be able to regulate the output currents, improve the dynamic response of the grid and achieve accurate power flow regulation at the point of common coupling (PCC) [10], [11].

In an islanded MG, it is crucial to achieve accurate power sharing while maintaining stable regulation of the MG voltage magnitude and frequency [12]. In the existing literatures, the droop control methods are widely adopted for a large/medium system, which mimics the behavior of a synchronous generator with no need of critical communication, to achieve the power sharing requirement eliminating an external high bandwidth communication links among the DG units [13]. Since the frequency is a global variable, the active power can be properly shared using the droop control, but the frequency and voltage amplitude deviations are inevitable in the steady-state conditions [14-17]. Moreover, the dynamic stability of the active power sharing controller is poor and the accuracy of power sharing is sensitive to the feeder impedance [18], [19].

In order to deal with the above problems in the islanded microgrid, a number of improved control methods have been proposed, which can be divided into improved droop control [20-25] and improved secondary control methods [26-34]. An improved virtual power-based control method with a unified rotation angle in the power transformation has been presented in [20], which can effectively realize power decoupling and then ensure system stability. However, since the voltage and current control loops, filters and loads are not considered in the small-signal model of the presented control strategy, the analysis of stability of the system is incomplete. A fuzzy logic-based improved droop control method is presented to balance the state of charge of DG energy storage systems [21]. However, the disturbance of the feeders and loads are not considered. An improved droop control method was proposed in [22] to share the DG currents and restore the bus voltage simultaneously without a centralized secondary controller. However, the communication lines are needed in this control strategy and the communication delay cannot be ignored. In [23], a fuzzy approach for intelligent model based droop control has been established to regulate the MG frequency and voltage amplitude simultaneously. However, it makes the control structure more complicated, and the influence of the unequal feeder impedance was not taken into account. In order to improve the dynamic performance of the MG, many literatures [24], [25] have presented a similar improved control method, which introduces derivative control into the droop controller. However, the derivative control may make the parallel DG system unstable, especially when the DG unit is under no-load conditions.

In addition, a distributed/centralized secondary control [26], [27] as the main trend methods, is used to restore the voltage amplitude and frequency to the rated values. A consensus-based secondary control strategy is presented in [28] to achieve accurate active power sharing in islanded MG with sparse communication lines. In [29], a two-layer cooperative control strategy is presented to simultaneously control both the voltage/frequency as well as the active/reactive power flows, where only own and neighbors' information of each DG unit are required. The improved secondary control strategies, such as the algorithms based on graph theory, predictive control and multi-agent system (MAS)-based control methods, are presented to enhance the dynamic stability and accuracy of the power sharing under changeable environmental conditions [30-32]. However, the low band-width communication (LBC) lines are inevitable to be utilized in these improved secondary control methods, and the output correction signals sent to the primary control are always accompanied by time delay and the control signals might be different from the theoretical analysis, which degrades the performance of the microgrid.

In [33], a gain scheduler method is utilized to decrease the influence on low bandwidth communication delay. In [34], a model predictive and a smith predictor-based controllers are presented to minimize the influence brought by the LBC lines in the secondary control. However, coefficients of controllers in these literatures are difficult to be obtained. Compared with the existing secondary control methods, a washout filter-based control method was presented without LBC lines and additional control loops [35]. However, the stability and dynamic behavior of the MG are not studied, and only simulation results are provided, which needs to be further analyzed.

In this paper, the equivalence between secondary control and washout filter-based control strategy are demonstrated, and the generalized washout filter-based power sharing scheme can be derived. Additionally, the physical meaning of parameters of the secondary controllers is discussed, emphasizing that the proportional and integral (PI) coefficients of the secondary controller are utilized to constitute a band-pass filter (BPF). Furthermore, a complete small-signal model of the generalized washout filter-based control method, considering the power stages, voltage and current controllers, LCL filters, feeder and load impedances, is proposed to design the control parameters of the calculated equivalent control model, and analyze the stability of the system. The feasibility and effectiveness of the proposed approach is validated by the hardware-in-the-loop (HIL) results obtained from the three parallel DG units-based islanded microgrid under unequal feeder impedance and load/DG disturbance conditions using the dSPACE 1006 control platform. Moreover, a down-scaled hardware prototype of islanded microgrid using two parallel-connected three-phase inverters is built and the experimental results are presented for verification. And the future research trends for the hierarchical controlled islanded microgrid is also discussed. The main contributions of this paper are summarized as follows.

1) The equivalence between secondary control and washout filter-based control method is verified in this paper, and the generalized washout filter - based power sharing strategy is derived to improve the dynamic stability of the islanded microgrid system. Moreover, the physical meaning of control parameters of secondary controllers is also discussed.
2) A complete small-signal model of the generalized washout filter-based control scheme is proposed to analyze the stability of the islanded MG system, and parameter design guidelines have been presented for the generalized washout filter-based control method, which can be also applied to the secondary and washout filter-based control methods.
3) The frequency and voltage amplitude can be restored to the rated values without any LBC lines. Moreover, compared with the existing control method, the maximum fluctuations of MG frequency and voltage amplitude are significantly decreased under disturbance conditions of DG units, load and feeder impedances.
4) Extensive HIL and experimental results validate the effectiveness and flexibility provided by the generalized washout filter-based control scheme. Moreover, the future research trends are summarized, and the proposed approach provides a new direction to study the possible equivalence in multiple microgrids clusters, in order to increase the robustness of the hierarchical controlled microgrids under LBC delays.

The rest of this paper is organized as follows. In Section II, the review of the secondary and washout filter-based control methods are presented. In Section III, the equivalence between the secondary control and washout filter-based methods are presented, and the generalized washout filter-based control scheme can be obtained. The detailed small-signal model of the generalized washout filter-based power sharing method is established to design the parameters in the derived control method and the stability of the islanded MG system is analyzed in Section IV. The HIL test results of the three DG-based islanded MG system are provided to verify the feasibility of the presented method in Section V. In Section VI, the test results from a down-scaled hardware prototype of islanded microgrid is presented, which verifies the correctness and effectiveness of the obtained equivalent control model. Section VII summarize the future research trends in hierarchical controlled microgrids. Finally, the concluding remarks are given in Section VIII.

II. Review of Secondary and Washout Filter-based Control strategies

In an islanded microgrid, a secondary control performs the function to eliminate the frequency and voltage deviations caused by the droop control algorithm, and maintain the stability of voltage and frequency of microgrid simultaneously [26], [27]. Additionally, to eliminate the impact of time delay caused by LBC lines in secondary controllers, a washout filter-based power sharing strategy without any communication link has been presented in [35].

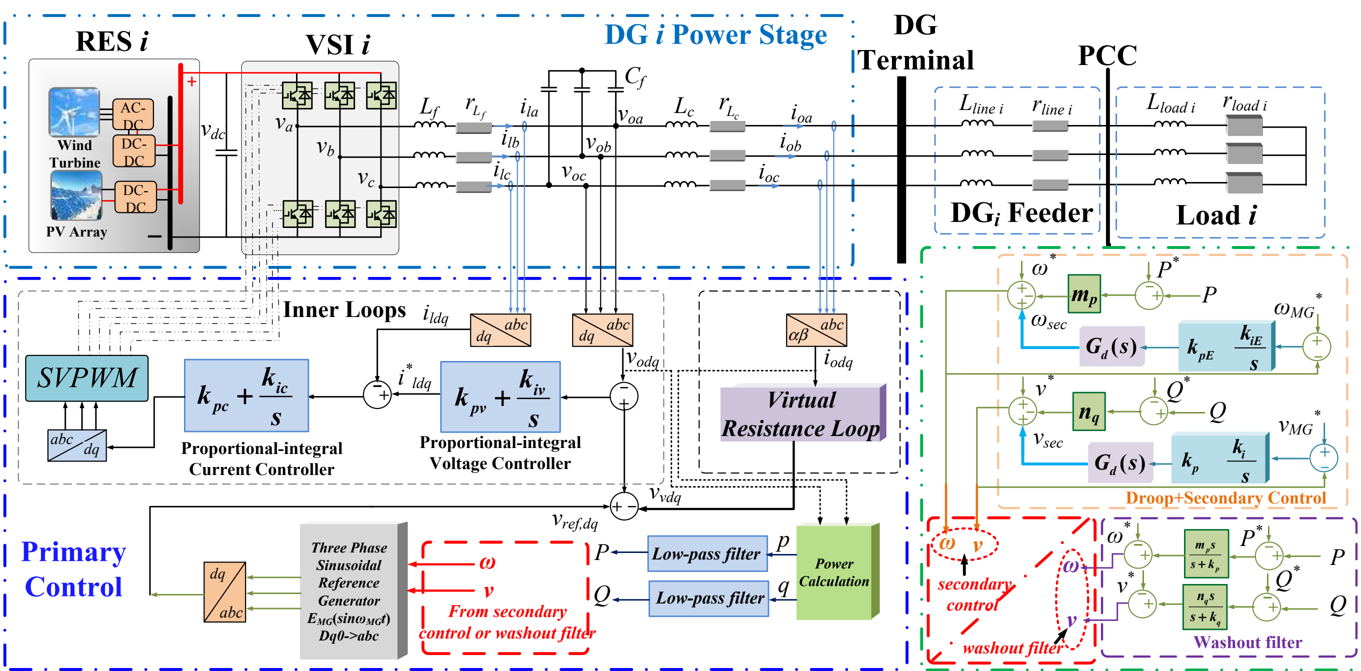

Fig. 1. Block diagram of the complete microgrid system including the secondary control or the washout filter-based control schemes.

Fig. 1 shows a power stage of a DG unit with secondary or washout filter-based controller for the interface inverter in an islanded mode. As depicted in Fig. 1, each DG unit can be connected to a predefined load or to the common bus directly, which can be considered as a subsystem of the MG. A brief description of secondary control and washout filter-based control strategy for the MG are outlined as follows [26-35].

A. The Secondary Control for Microgrids

In islanded MG, the foundation of control loops of each DG unit must be established to stabilize the network and achieve a good power sharing among the DG units [27]. Therefore, the classical (*P*/*f*, *Q*/*V*) droop control scheme in large systems (high voltage) and medium systems (medium voltage) is introduced, which can be defined as [36]:

$$\begin{cases} \omega = \omega^* - m_p P \\ v = v^* - n_q Q \end{cases} \quad (1)$$

where ω and v represent the frequency and amplitude of the output voltage. ω^* and v^* are the rated angular frequency and voltage, respectively. P and Q are the measured average active and reactive powers through a low-pass filter, and m_p and n_q are the frequency and amplitude droop coefficients, respectively.

The droop controller is responsible for adjusting the frequency and the amplitude of the voltage reference according to the active and reactive powers (P and Q) [26], and to achieve the active power sharing among multiple DG units. However, the deviations of the frequency and voltage amplitude are inevitable, and the dynamic stability of the active power sharing is poor with the disturbances of loads and feeder dynamics [26-34]. Therefore, in order to solve the problems caused by the conventional droop control, a secondary control can be used to eliminate the frequency and voltage deviations, and improve the stability of the MG [37], [38].

Fig. 1 depicts the details of a secondary control structure, which is realized by using low bandwidth communication (LBC) among the multiple DG units. The secondary control consists of a proportional–integral (PI) controller, and the frequency and amplitude restoration compensators can be derived as [27]:

$$\begin{cases} \omega_{\sec} = k_{p\omega}\left(\omega_{MG}^* - \omega\right) + k_{i\omega}\int\left(\omega_{MG}^* - \omega\right)dt \\ v_{\sec} = k_{pE}\left(v_{MG}^* - v\right) + k_{iE}\int\left(v_{MG}^* - v\right)dt \end{cases} \quad (2)$$

where $k_{p\omega}$, $k_{i\omega}$, k_{pE} and k_{iE} are the control parameters of the PI compensator of the frequency and voltage restoration control, respectively. The errors between measured angular frequency (ω) and reference angular frequency (ω_{MG}^*) are processed by the PI compensator and then sent the control signal ω_{sec} to all the DG units to restore the frequency of MG to the rated value. The control signal v_{sec} is also sent to primary control level to remove the voltage difference brought by the droop controller.

Notably, the centralized secondary control architecture requires each DG unit to communicate with a central controller, or requires all DGs to communicate with all others directly [26], [27]. Therefore, a MG will be unstable when the output frequency and voltage amplitude correction signals sent to primary control are different to the theoretical values, due to the low band-width communication (LBC) delays and data drop in the communication lines. Therefore, the secondary control for active power sharing should be further improved to get an accurate and robust active power sharing for the MGs, and decrease the impact of the LBC delays and data drop.

B. Washout Filter-based Power Sharing Strategy for Islanded Microgrids

To eliminate the impact of time delay caused by the LBC lines and restore the frequency and voltage amplitude to the rated values simultaneously, a washout filter-based power sharing has been presented in [35] without any communication links and additional control loops as follows:

$$\begin{cases} \omega = \omega^* - \dfrac{m_p s}{s + k_p}\left(P - P^*\right) \\ v = v^* - \dfrac{n_q s}{s + k_q}\left(Q - Q^*\right) \end{cases} \quad (3)$$

where k_p and k_q are the control parameters of the washout filter. By using the control strategy as indicated in (3), voltage and frequency deviations can be prevented without the need for the secondary level control and extra controllers, where the droop coefficients are replaced by washout filters.

Notice that the washout filter-based control strategy is an equivalent secondary controller, which will be analyzed in next section. Moreover, the physical meaning of parameters of the secondary controllers will also be discussed in Section III.Equivalence Between secondary and Washout Filter-based controllers

Usually, frequency and voltage deviations from the nominal values due to the droop algorithm can be compensated by a secondary control [26-34]. Referring to Fig. 1, the output voltage amplitude and frequency of the droop controller can be obtained as:

$$\begin{cases} \omega = \omega^* - m_p(\underbrace{p \cdot G_{LPF}(s)}_{P} - P^*) + \omega_{\sec} \\ v = v^* - n_q(\underbrace{q \cdot G_{LPF}(s)}_{Q} - Q^*) + v_{\sec} \end{cases} \quad (4)$$

where p and q are instantaneous active and reactive powers, respectively. In the secondary voltage amplitude control loop, $v_{\sec}$ can be obtained as:

$$\begin{aligned} v_{\sec} &= (v_{MG}^* - v) \cdot G_{v,\sec}(s) \cdot G_d(s) \\ &= (v_{MG}^* - (v^* - n_q(q \cdot G_{LPF}(s) - Q^*) + v_{\sec})) \\ &\quad \cdot G_{v,\sec}(s) \cdot G_d(s) \end{aligned} \quad (5)$$

where G_d(s) is the transfer function of unknown LBC delay. The transfer function $G_{LPF}(s)$, $G_{v,\sec}(s)$ and $G_{\omega,\sec}(s)$ are defined as follows:

$$\begin{cases} G_{v,\sec}(s) = k_{pE} + \dfrac{k_{iE}}{s} \\ G_{\omega,\sec}(s) = k_{p\omega} + \dfrac{k_{i\omega}}{s} \\ G_{LPF}(s) = \dfrac{\omega_c}{s + \omega_c} \end{cases} \quad (6)$$

where ω_c is the cut-off frequency of the low-pass filter (LPF).

Moreover, the LBC delay is uncertain in the secondary controlled islanded microgrid, which may affect the stability of the system. Under ideal circumstances, the transfer function of LBC delay $G_d(s)$ is considered to be unity. The reference voltage of the microgrid v^*_{MG} is set to be v^* and the reference angular frequency of MG ω^*_{MG} is set to be ω^*. Besides, the reference powers P^* and Q^* are set to be zero for islanded microgrid [39], [40].

Therefore, (5) can be simplified as:

$$v_{\sec} = \frac{n_q}{\frac{1}{G_{v,\sec}}+1}(Q\cdot G_{LPF}(s)-Q^*) \tag{7}$$

Combining (4) and (7), the output voltage can be obtained as:

$$\begin{aligned} v &= v^* - n_q(Q\cdot G_{LPF}(s)-Q^*) + \frac{n_q}{\frac{1}{G_{v,\sec}}+1}(Q\cdot G_{LPF}(s)-Q^*) \\ &= v^* - n_q\cdot\frac{\omega_c}{s+\omega_c}\cdot\frac{1}{G_{v,\sec}+1}\cdot q \\ &= v^* - \frac{n_q}{k_{pE}+1}\cdot\underbrace{\underbrace{\frac{\omega_c}{s+\omega_c}}_{low-pass}\cdot\underbrace{\frac{s}{s+\frac{k_{iE}}{k_{pE}+1}}}_{high-pass}}_{band-pass\ filter}\cdot q \end{aligned} \tag{8}$$

Besides, the angular frequency can be derived as:

$$\omega=\omega^* - \frac{m_p}{k_{p\omega}+1}\cdot\underbrace{\underbrace{\frac{\omega_c}{s+\omega_c}}_{low-pass}\cdot\underbrace{\frac{s}{s+\frac{k_{i\omega}}{k_{p\omega}+1}}}_{high-pass}}_{band-pass\ filter}\cdot p \tag{9}$$

Therefore, from (8) and (9), a generalized washout filter-based power sharing strategy can be obtained. Note that a washout filter-based control strategy can be achieved when the conditions $k_{p\omega}=k_{pE}=0$, $k_{i\omega}=k_p$, and $k_{iE}=k_q$ are satisfied. Moreover, it can be concluded that the washout filter-based power sharing strategy is intrinsically an ideal secondary control without communication delay.

As can be seen in (8) and (9), cut-off frequencies ω_{hE} and $\omega_{h\omega}$ of high-pass filter (HPF) are constituted by the proportional and integral coefficients of the secondary controller, where ω_{hE} and $\omega_{h\omega}$ are defined as:

$$\omega_{hE} = \frac{k_{iE}}{k_{pE}+1},\ \omega_{h\omega} = \frac{k_{i\omega}}{k_{p\omega}+1} \tag{10}$$

From (2), (3), (8), (9) and (10), it can be observed that a generalized washout filter-based power sharing strategy are formed by band-pass filter (BPF), realized by cascading LPF and HPF. Therefore, the parameters of washout-based control method are mainly affected by the cut-off frequencies of BPF. The frequency characteristics of a BPF in the washout filter-based controlled islanded MG can be shown in Fig. 2, where f_{high} and f_{low} represent the cut-off frequency of the high-pass and low-pass filter, respectively, and f_{center} is the center frequency of the BPF.

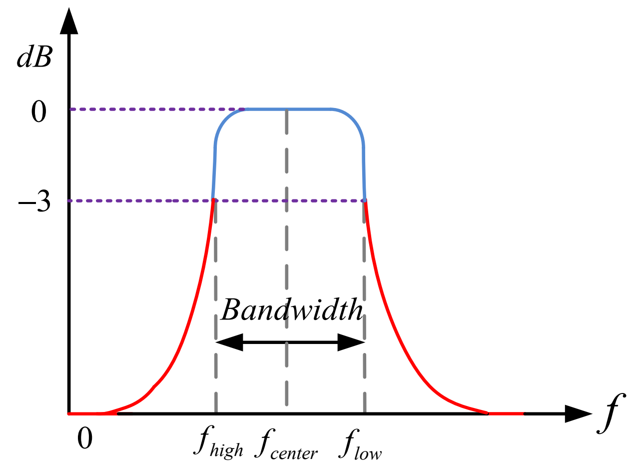

Fig. 2.The frequency characteristics of a BPF in the secondary controlled islanded MG.

The cut-off frequency is defined as the frequency when the power of a signal is at its -3 dB attenuation point [41], [42]. In this way, a good performance of secondary control can be ensured, when the cut-off frequency of the high-pass filter satisfies the following conditions:

$$\frac{k_{iE}}{k_{pE}+1} < \omega_c,\ \frac{k_{i\omega}}{k_{p\omega}+1} < \omega_c \tag{11}$$

Equation (11) gives a restrictive condition to design the parameters in a washout filter-based or secondary control strategies. Moreover, the physical meaning of parameters of secondary controllers is used to form a BPF, which has not been discussed in the existing literatures. If an islanded MG system with the secondary controllers does not satisfy the conditions imposed by the cut-off frequency restraint as represented by (11), the power signals p and q passing through ill-conditioned BPFs will be augmented and oscillating. In other words, droop control may be ineffective, and the dynamic stability of the whole system cannot be guaranteed. Moreover, the stability of islanded MGs with generalized washout filter-based approach, and the parameters design guidelines of this equivalent control model will be analyzed in next section.

III. Small-Signal Model for the Generalized Washout Filter-Based Control Method

This section presents the small-signal model of the generalized washout filter-based power sharing strategy for the islanded microgrid, emphasizing the design of the control parameters, and the stability analysis of the MG.

A. Power Controller Loops

The linearized small-signal models of the active and reactive power controllers can be written as [43]:

$$\begin{cases} \Delta \dot{P} = -\omega_c\Delta P + \omega_c(i_{od}\Delta v_{od} + i_{oq}\Delta v_{oq} + v_{od}\Delta i_{od} + v_{oq}\Delta i_{oq}) \\ \Delta \dot{Q} = -\omega_c\Delta Q + \omega_c(-i_{oq}\Delta v_{od} + i_{od}\Delta v_{oq} + v_{oq}\Delta i_{od} - v_{od}\Delta i_{oq}) \end{cases} \tag{12}$$

where "Δ" is the small signal perturbation.

By linearizing (8) and (9), the small signal dynamics of the generalized washout filter-based control equations can be obtained as:

$$\begin{cases} \Delta\omega = -\dfrac{k_{i\omega}}{k_{p\omega}+1}\Delta\omega - \dfrac{m_p}{k_{p\omega}+1}\Delta P \\ \Delta v = -\dfrac{k_{i\omega}}{k_{p\omega}+1}\Delta v - \dfrac{m_p}{k_{p\omega}+1}\Delta Q \end{cases} \tag{13}$$

Besides, voltage phase angle and amplitude expressions in the d-q coordinate system are denoted as [44-46]:

$$\delta = \arctan\left(\frac{v_d}{v_q}\right),\ v = \sqrt{v_d^2 + v_q^2} \tag{14}$$

where v_d and v_q are the projection of the output voltage v of power controllers on two perpendicular rotating d and q axes, respectively, and the phase angle δ between v and v_d is represented by The following equation can be obtained [44-46]:

$$\begin{cases} \Delta\delta = -\dfrac{v_q}{v_d^2+v_q^2}\Delta v_d + \dfrac{v_d}{v_d^2+v_q^2}\Delta v_q \\ \Delta v = \dfrac{v_d}{\sqrt{v_d^2+v_q^2}}\Delta v_d + \dfrac{v_q}{\sqrt{v_d^2+v_q^2}}\Delta v_q \\ \Delta v = \dfrac{v_d}{\sqrt{v_d^2+v_q^2}}\Delta v_d + \dfrac{v_q}{\sqrt{v_d^2+v_q^2}}\Delta v_q \end{cases} \tag{15}$$

By using $\Delta\omega(s)=s\Delta\delta(s)$, and combining (12), (13) and (15), the small-signal model of power stage of each DG inverter can be obtained as:

$$\begin{bmatrix} \Delta\omega \\ \Delta P \\ \Delta Q \\ \Delta v_d \\ \Delta v_q \end{bmatrix} = [\mathbf{T_{BPF}}]_{5\times5} \begin{bmatrix} \Delta\omega \\ \Delta P \\ \Delta Q \\ \Delta v_d \\ \Delta v_q \end{bmatrix} \tag{16}$$

where the complete matrix $\mathbf{T_{BPF}}$ is given in Appendix A.

B. Equations of Voltage and Current Controllers and LCL Filters

The output reference current and the linearized small-signal state-space form of the voltage controller, where the standard PI controllers are used, are represented by (17) and (18), respectively [43]:

$$\begin{bmatrix} \Delta i_{ld}^* \\ \Delta i_{lq}^* \end{bmatrix} = [\mathbf{C_V}]\begin{bmatrix} \Delta\phi_d \\ \Delta\phi_q \end{bmatrix} + [\mathbf{D_{V1}}]\begin{bmatrix} \Delta v_d \\ \Delta v_q \end{bmatrix} + [\mathbf{D_{V2}}]\begin{bmatrix} \Delta i_{ld} \\ \Delta i_{lq} \\ \Delta v_{od} \\ \Delta v_{oq} \\ \Delta i_{od} \\ \Delta i_{oq} \end{bmatrix} \tag{17}$$

$$\begin{bmatrix} \Delta\phi_d \\ \Delta\phi_q \end{bmatrix} = [\mathbf{0_V}]\begin{bmatrix} \Delta\phi_d \\ \Delta\phi_q \end{bmatrix} + [\mathbf{B_{V1}}]\begin{bmatrix} \Delta v_d \\ \Delta v_q \end{bmatrix} + [\mathbf{B_{V2}}]\begin{bmatrix} \Delta i_{ld} \\ \Delta i_{lq} \\ \Delta v_{od} \\ \Delta v_{oq} \\ \Delta i_{od} \\ \Delta i_{oq} \end{bmatrix} \tag{18}$$

where the complete matrix $\mathbf{C_V}$, $\mathbf{D_{V1}}$, $\mathbf{D_{V2}}$ and $\mathbf{B_{V2}}$ are given in Appendix A. $\mathbf{B_{V1}}$ is a second-order identity matrix and $\mathbf{0_V}$ is a second-order zero matrix. The state variables i_{ld}^*, i_{lq}^* and i_{ld}, i_{lq} are the dq-axis commanded filter inductor currents and inverter currents, respectively. The state variables v_{od}, v_{oq} and i_{od}, i_{oq} are the dq-axis actual output voltages and currents of inverters, respectively. ϕ_d and ϕ_q are introduced to establish the small-signal model of the voltage controller.

$$\begin{bmatrix} \Delta v_{id}^* \\ \Delta v_{iq}^* \end{bmatrix} = [\mathbf{C_C}]\begin{bmatrix} \Delta\gamma_d \\ \Delta\gamma_q \end{bmatrix} + [\mathbf{D_{C1}}]\begin{bmatrix} \Delta i_{ld}^* \\ \Delta i_{lq}^* \end{bmatrix} + [\mathbf{D_{C2}}]\begin{bmatrix} \Delta i_{ld} \\ \Delta i_{lq} \\ \Delta v_{od} \\ \Delta v_{oq} \\ \Delta i_{od} \\ \Delta i_{oq} \end{bmatrix} \tag{19}$$

$$\begin{bmatrix} \Delta\gamma_d \\ \Delta\gamma_q \end{bmatrix} = [\mathbf{0_C}]\begin{bmatrix} \Delta\gamma_d \\ \Delta\gamma_q \end{bmatrix} + [\mathbf{B_{C1}}]\begin{bmatrix} \Delta i_{ld}^* \\ \Delta i_{lq}^* \end{bmatrix} + [\mathbf{B_{C2}}]\begin{bmatrix} \Delta i_{ld} \\ \Delta i_{lq} \\ \Delta v_{od} \\ \Delta v_{oq} \\ \Delta i_{od} \\ \Delta i_{oq} \end{bmatrix} \tag{20}$$

The output reference voltage and the linearized small-signal state-space form of PI current controller are achieved by (19) and (20), respectively [47], where the complete matrix $\mathbf{C_C}$, $\mathbf{D_{C1}}$, $\mathbf{D_{C2}}$ and $\mathbf{B_{C2}}$ are presented in Appendix A. $\mathbf{B_{C1}}$ is a second-order identity matrix and $\mathbf{0_C}$ is a second-order zero matrix. The state variables v_{id}^* and v_{iq}^* are the dq-axis commanded voltages. γ_d and γ_q are used for making convenience to establish the small-signal model of the current controller.

Besides, the small-signal model of the output LCL filter can be represented with the following state equations [48]:

$$\begin{bmatrix} \Delta i_{ld} \\ \Delta i_{lq} \\ \Delta v_{od} \\ \Delta v_{oq} \\ \Delta i_{od} \\ \Delta i_{oq} \end{bmatrix} = [\mathbf{A_{LCL}}]\begin{bmatrix} \Delta i_{ld} \\ \Delta i_{lq} \\ \Delta v_{od} \\ \Delta v_{oq} \\ \Delta i_{od} \\ \Delta i_{oq} \end{bmatrix} + [\mathbf{B_{LCL1}}]\begin{bmatrix} \Delta v_{id} \\ \Delta v_{iq} \end{bmatrix} + [\mathbf{B_{LCL2}}]\begin{bmatrix} \Delta v_{bd} \\ \Delta v_{bq} \end{bmatrix} + [\mathbf{B_{LCL3}}][\Delta\omega] \tag{21}$$

where the complete matrix $\mathbf{A_{LCL}}$, $\mathbf{B_{LCL1}}$, $\mathbf{B_{LCL2}}$ and $\mathbf{B_{LCL3}}$ are given in Appendix A. The state variables v_{bd} and v_{bq} are the dq-axis voltages at the point of common coupling (PCC).

C. Equations for the Distribution Lines and Loads

The generic RL loads of the MG system are chosen in this paper, and the state equations of the RL load connected at PCC are depicted by (22) as [49].

The state variable i_{loadD}, i_{loadQ} are the dq-axis load currents at the PCC. r_{load} and L_{load} are the load resistance and inductance, respectively.

Besides, the resistance and inductance of the distribution line connected between the ith DG unit (DG$_i$) and the jth DG unit (DG$_j$) are represented as follows [47-50]:

$$\begin{bmatrix}\Delta i_{loadD}\\ \Delta i_{loadQ}\end{bmatrix}=\begin{bmatrix}-\dfrac{r_{load}}{L_{load}} & \omega_0\\ -\omega_0 & -\dfrac{r_{load}}{L_{load}}\end{bmatrix}\begin{bmatrix}\Delta i_{loadD}\\ \Delta i_{loadQ}\end{bmatrix}+\begin{bmatrix}\dfrac{1}{L_{load}} & 0\\ 0 & \dfrac{1}{L_{load}}\end{bmatrix}\begin{bmatrix}\Delta b_D\\ \Delta b_Q\end{bmatrix}+\begin{bmatrix}I_{loadQ}\\ -I_{loadD}\end{bmatrix}[\Delta\omega] \qquad (22)$$

$$\begin{bmatrix}\Delta i_{lineDij}\\ \Delta i_{lineQij}\end{bmatrix}=\begin{bmatrix}-\dfrac{r_{line}}{L_{line}} & \omega_0\\ -\omega_0 & -\dfrac{r_{line}}{L_{line}}\end{bmatrix}\begin{bmatrix}\Delta i_{lineDij}\\ \Delta i_{lineQij}\end{bmatrix}+\begin{bmatrix}\dfrac{1}{L_{line}} & 0 & -\dfrac{1}{L_{line}} & 0\\ 0 & \dfrac{1}{L_{line}} & 0 & -\dfrac{1}{L_{line}}\end{bmatrix}\begin{bmatrix}\Delta b_{Di}\\ \Delta b_{Qi}\\ \Delta b_{Dj}\\ \Delta b_{Qj}\end{bmatrix}+\begin{bmatrix}I_{lineQ}\\ -I_{lineD}\end{bmatrix}[\Delta\omega] \qquad (23)$$

where the state variables $i_{lineDij}$ and $i_{lineQij}$ are the dq-axis line currents between the ith and jth bus. r_{line} and L_{line} are the resistance and inductance of distribution lines, respectively.

Moreover, the virtual resistor is assumed to be connected at the inverter bus and the following equation can be obtained by using Kirchhoff's Voltage Law (KVL) [49], [50].

$$\begin{cases} v_{bD}=r_N\left(i_{oD}-i_{loadD}+i_{lineDij}\right)\\ v_{bQ}=r_N\left(i_{oQ}-i_{loadQ}+i_{lineQij}\right)\end{cases} \qquad (24)$$

where r_N is the virtual resistor connected at the ith bus, which is used to increase the dynamic stability of the system and make convenience to establish the small-signal model of the system.

D. Reference Frame Transformation

Note that each DG operates in its own local reference frame. Therefore, the individual reference frame of a DG needs to be taken as a common reference frame and the rest of all DG units including network and loads are transformed onto this reference frame as defined in (25) and (26) [51], [52]:

$$\begin{bmatrix}x_D\\ x_Q\end{bmatrix}_{global}=\begin{bmatrix}\cos\theta & \sin\theta\\ -\sin\theta & \cos\theta\end{bmatrix}\begin{bmatrix}x_d\\ x_q\end{bmatrix}_{local} \qquad (25)$$

$$\begin{bmatrix}x_d\\ x_q\end{bmatrix}_{local}=\begin{bmatrix}\cos\theta & -\sin\theta\\ \sin\theta & \cos\theta\end{bmatrix}\begin{bmatrix}x_D\\ x_Q\end{bmatrix}_{global} \qquad (26)$$

where the state variables x_d, x_q and x_D, x_Q are the dq-axis local and global variables, respectively.

E. Linearized Model of the Complete MG System

From the above analysis, it can be deduced that each DG contains 17 states and each model of line connected between two DG units contains two states. A total number of 36 state variables contained in an islanded MG system considering two parallel DG units is taken as an example:

$$\left[\Delta\mathbf{X}\right]=\left[\Delta\mathbf{X}_1\ \Delta\mathbf{X}_{1,2}\ \Delta\mathbf{X}_2\right]^T=\mathbf{A_{sys}}\left[\Delta\mathbf{X}\right] \qquad (27)$$

where $\Delta\mathbf{X}_1$, $\Delta\mathbf{X}_{1,2}$ and $\Delta\mathbf{X}_2$ are represented by (28), (29) and (30), respectively:

$$\begin{aligned}\left[\Delta\mathbf{X}_1\right]=[&\Delta\omega_1\ \Delta P_1\ \Delta Q_1\ \Delta v_{d1}\ \Delta v_{q1}\ \Delta\phi_{d1}\ \Delta\phi_{q1}\ \Delta\gamma_{d1}\ \Delta\gamma_{q1}\\ &\Delta i_{ld1}\ \Delta i_{lq1}\ \Delta v_{od1}\ \Delta v_{oq1}\ \Delta i_{od1}\ \Delta i_{oq1}\ \Delta i_{loadD1}\ \Delta i_{loadQ1}]^{\mathrm{T}}\end{aligned} \qquad (28)$$

$$\left[\Delta\mathbf{X}_{1,2}\right]=[\Delta i_{lineD1,2}\quad \Delta i_{lineQ1,2}]^{\mathrm{T}} \qquad (29)$$

$$\begin{aligned}\left[\Delta\mathbf{X}_2\right]=[&\Delta\omega_2\ \Delta P_2\ \Delta Q_2\ \Delta v_{d2}\ \Delta v_{q2}\ \Delta\phi_{d2}\ \Delta\phi_{q2}\ \Delta\gamma_{d2}\ \Delta\gamma_{q2}\\ &\Delta i_{ld2}\ \Delta i_{lq2}\ \Delta v_{od2}\ \Delta v_{oq2}\ \Delta i_{od2}\ \Delta i_{oq2}\ \Delta i_{loadD2}\ \Delta i_{loadQ2}]^{\mathrm{T}}\end{aligned} \qquad (30)$$

Fig. 3 shows a sparsity pattern of $\mathbf{A_{sys}}$, where seven regions are depicted in the matrix diagram and the nonzero elements are distributed across the diagonal of the matrix. Moreover, regions 1, 2 and 3 are formed by DG_1, while regions 5, 6 and 7 are formed by DG_2. And region 4 is formed by the distribution line between DG_1 and DG_2. Region 1 and 5 are formed based on (16), (18) and (20), which contain power stages, and the voltage and current control loops. Besides, the angular frequency of DG_1 is set as the reference angular frequency for the DG_2. Region 2 and 6 are formed by using (21), which contains LCL filters of each DG unit. Region 3 and 7 are formed by the loads, and virtual resistors are depicted in region 4. Therefore, a new sparsity state matrix diagram can be obtained, where additional patterns identical to those in regions 1, 2, 3 and 4 are located on the diagonal of the matrix following the sparsity pattern of DG_2, when other DG units are added to the MG system.

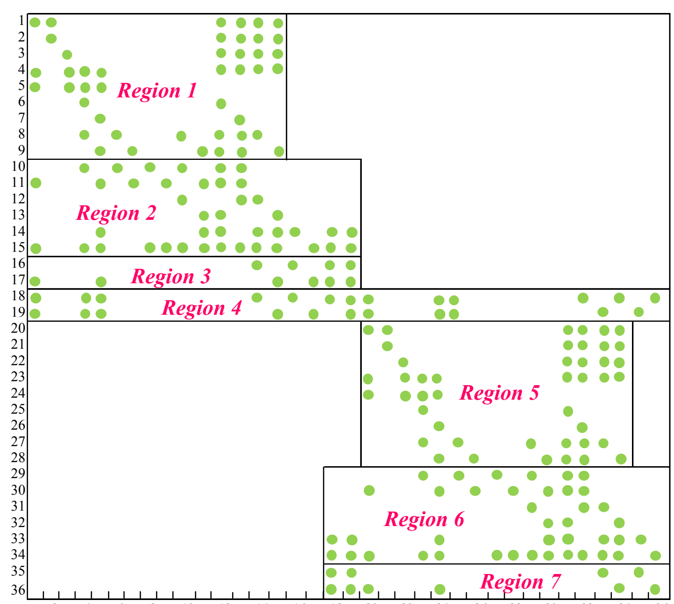

Fig. 3. Sparsity pattern of the state matrix A_{sys}.

F. Modeling Results and Small-Signal Stability Analysis

A complete model of the test system was established by a sparsity state matrix $\mathbf{A_{sys}}$ presented in (27), and the complete eigenvalues of the system can be calculated, by using the initial conditions of the system in Table I.

Fig. 4 shows the eigenvalues of the MG system distributed in a large range of frequency scale, which can be divided into three different clusters due to the time-scale separation among the different control loops. The cluster "3" appeared in high-frequency modes are sensitive to the distribution of the state variables of LCL filters and the impedance of feeders, while the medium-frequency modes in cluster "2" are affected by the inner control loops. Moreover, it can be observed that the low-frequency modes shown in cluster "1" are sensitive to the state variables (elements in matrix $\mathbf{T_{BPF}}$) of the generalized washout filter-based power controller, which is crucial for analyzing the stability of the microgrid system.

Fig. 5 shows a method for the selection of the parameter k_{iE} of the generalized washout filter-based power controllers. The eigenvalue loci of cluster "1" and "2" (the real component is greater than -400) of state matrix $\mathbf{A_{sys}}$ change along with the increasing of ω_{hE} (where ω_{hE}=k_{iE}/(k_{pE}+1)) when the k_{pE}=0.001 and other parameters are chosen as the initial conditions.

From Fig. 5, it can be observed that a pair of dominant eigenvalues in cluster 1 and 2 will go across the imaginary axis, which indicates that the system loses stability according to the first Lyapunov's theorem [49]. Therefore, the cut-off frequency ω_{hE} of the high-pass filter in (10) should be limited and then the corresponding parameter k_{iE}=0.6 can be determined. In addition, other unknown parameters can be easily designed using the similar approach by varying the parameter of controllers while keeping other parameters fixed.

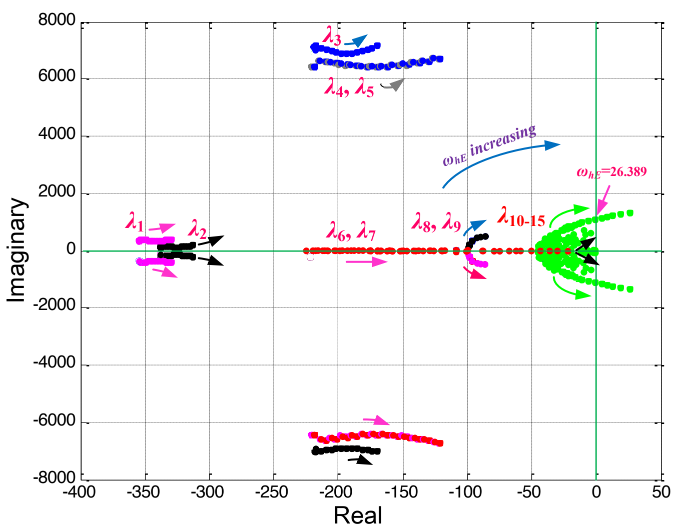

Fig.5. Root locus diagram of parallel DG-based microgrid system with the change of ω_{hE}.

TABLE I
INITIAL CONDITIONS AND SYSTEM PARAMETERS

Initial Conditions and System Parameters	Values
LCL filter	L_f= L_c=1.8 mH and C_f=25 µF r_{Lf}=0.1Ω and r_{Lc}=0.01Ω
DC link voltage	650 V
Switching frequency	10kHz
DG feeder	Feeder 1 inductance and resistance L_{line1}=2.2mH r_{line1}=0.2Ω Feeder 2 inductance and resistance L_{line2}=0.8mH r_{line2}=0.1Ω
Output Voltage	DG1: 325.26V DG2: 325.26V DG3:325.26V
PCC Voltage	DG1: 322.79V DG2: 322.79V DG3:322.79V
Voltage and Current Control Parameters	Values
k_{pv}, k_{iv}	0.175, 200
k_{pc}, k_{ic}	1.8, 131
Power Control Parameters	Values
$k_{p\omega}$, $k_{i\omega}$	0.005, 4
k_{pE}, ω_c	0.001, 10π
m_p, n_q	10e-4, 10e-4
k_p, k_q	2, 2
Load Parameters	Values
DG load	Loads inductance and resistance L_{load1}=L_{load2}=L_{load3}=720 mH r_{load1}= r_{load2}=r_{load3}=5Ω

IV. HARDWARE-IN-THE-LOOP RESULTS

The conventional droop control method, secondary control considering LBC delay, the washout filter-based strategy and generalized washout filter-based power sharing scheme are implemented on an islanded MG consists of three parallel DG units, as shown in Fig. 6, in order to confirm equivalence between secondary control and washout filter-based control strategies.

In Fig. 6, the MG system operates on the unequal feeder impedance and resistive-inductive load conditions. Besides, the different load and feeder impedance conditions are controlled by the switch (SW) 1, 2, 3 and 4. Each DG unit is connected to an LCL filter to eliminate the PWM switching harmonics, and disturbances of DG units, load and feeder impedances are tested to investigate the performance of the active power sharing, frequency and voltage regulation of the different control strategies. The complete parameters of the test system are given in Table I. The conventional droop controller and secondary control are compared with the generalized washout filter-based control scheme, which are implemented in Matlab/ Simulink, with measurements recorded through a dSPACE 1006 based real-time digital simulator in this section.

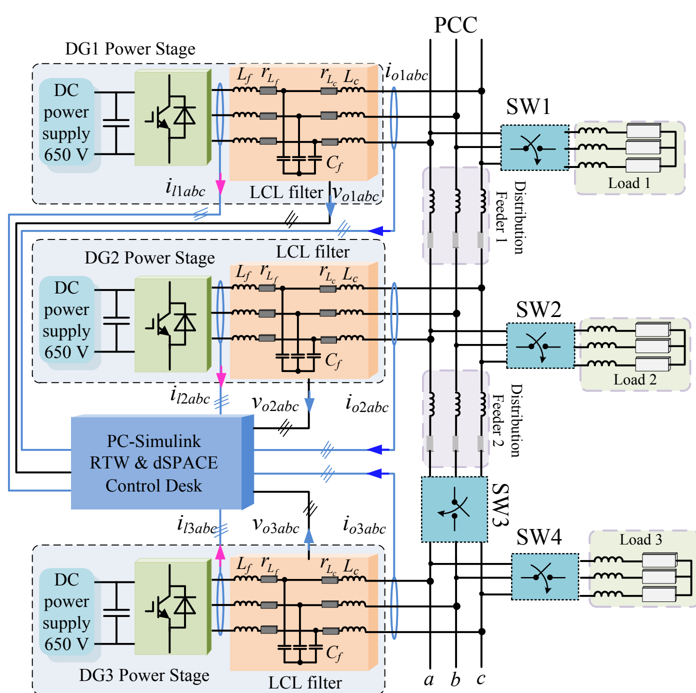

Fig. 6. Structure of the paralleled-connected DG units in an islanded MG.

A. *Performance of the Conventional Droop Controller*

In Fig. 7, the active power, frequency and voltage amplitude from each inverter operating under a conventional droop control scheme are shown.

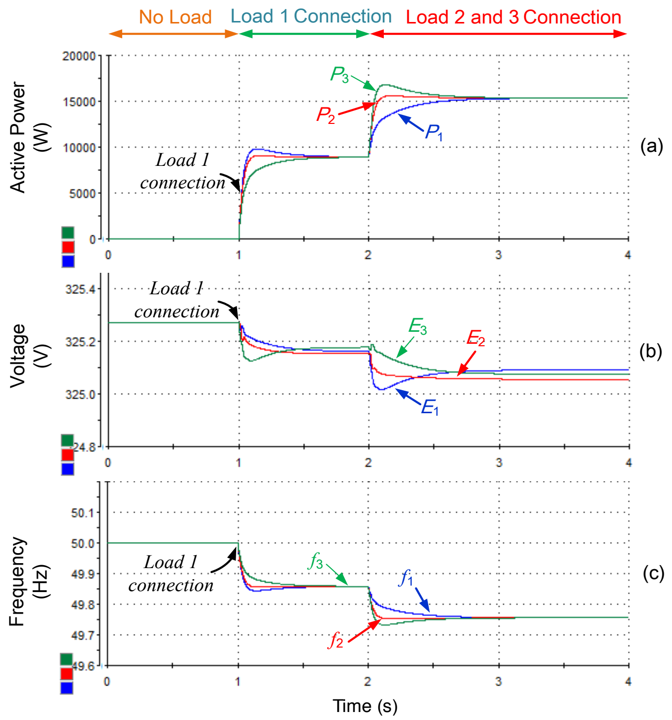

Fig. 7. Dynamic response of the islanded microgrid for the conventional droop control under load disturbance conditions. a) active power of each DG unit. b) output voltage of each DG unit. c) frequency of the microgrid.

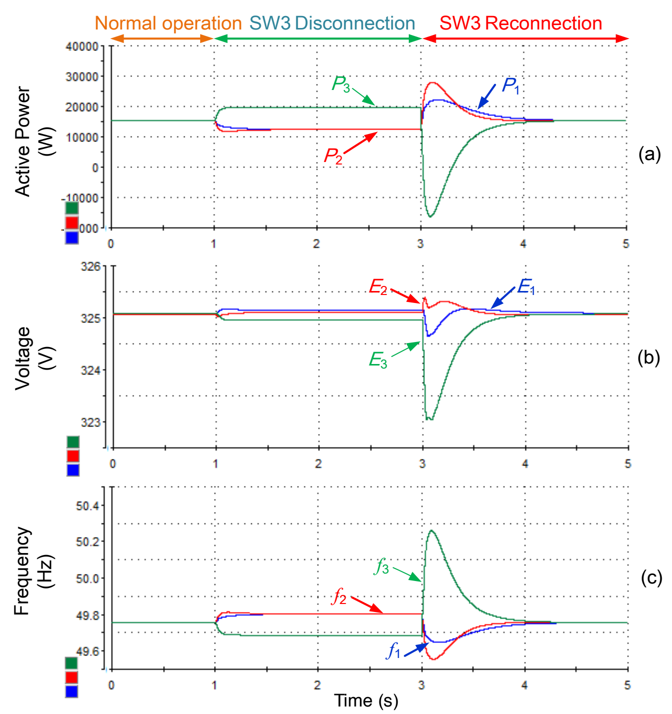

Fig. 8. Dynamic response of the islanded microgrid for the conventional droop control under feeder disturbance conditions. a) active power of each DG unit. b) output voltage of each DG unit. c) frequency of the microgrid.

Initially, the microgrid operates in the steady-state under no load condition. At t=1s, the load 1 is connected to the microgrid, and the droop mechanism ensures that the active power is shared among the inverters. However, the steady-state errors about 0.14 Hz in the frequency and 0.11 V in the voltage amplitude can be observed. At t=2s, all loads are connected to the microgrid, and the larger voltage and frequency deviations about 0.18V and 0.24 Hz, respectively, are caused by the droop control.

Another drawback of the conventional droop control is that the dynamic stability of active power is poor, as shown in Fig.8. In this scenario, the SW3 is disconnected at t=1s and reconnected at t=3s, and only DG_3 supply the energy to the load "3" during this time. When SW3 is reconnected, it can be observed that the active power, frequency and voltage amplitude differences of DG_3 reach to 200%, 1% and 0.6% of nominal value, respectively. Therefore, the conventional droop control should be further improved to get an accurate and robust active power sharing for MGs.

B. *Performance of the Secondary Control Considering the LBC Delays and Communication Failure*

The performance of the secondary control strategy applied to a microgrid has been depicted in Fig. 9 and 10. As seen in Fig. 9 and 10, the response time and LBC delay are represented by τ and τ_d, respectively. In secondary controlled microgrid, the LBC lines are utilized to send secondary control signals to the primary control level of each DG, in order to restore the frequency and voltage amplitude to the rated values.

In Fig. 9, the secondary control is activated at t=1s, and the voltage and frequency deviation need a time delay to be eliminated, where the LBC delay τ_d=120 ms is considered. To create a realistic failure scenario, at t=3s, load 2 and 3 are connected but the LBC lines are deactivated. It is undesirable that the frequencies of each DG unit drop for 0.1 Hz in the steady-state. Moreover, the voltage differences of the DG_1, DG_2 and DG_3 drop for 0.135V, 0.149V and 0.175V in the steady-state, respectively.

Fig. 10 shows a scenario that the SW3 is connected at t=1s and disconnected at t=3s. Besides, the secondary control is activated at t=0.5s and τ_d=120 ms is considered in this situation. It can be observed that the active power, frequency and voltage amplitude fluctuation will occur, because the feeder disturbance and LBC delays exist simultaneously in the MG system.

C. *Performance of the Washout Filter-Based Control Method*

The dynamic response of the washout filter-based control for islanded microgrid system are shown in Figs. 11 and 12, where the conditions k_p=2, k_q=2 are satisfied. Initially, the microgrid operates in the steady-state under no load condition and the load 1 is connected to the MG system at t=1s, as shown in Fig.11. Although transient errors about 0.524 Hz in the frequency and about 0.613V in the voltage amplitude can be obtained, the washout filter-based control strategy is able to eliminate the voltage and frequency deviations in about 1.59s. At t=3s, when the load 2 and 3 are connected to the MG system, the frequency and voltage can also be restored to the rated values within 1.5s.

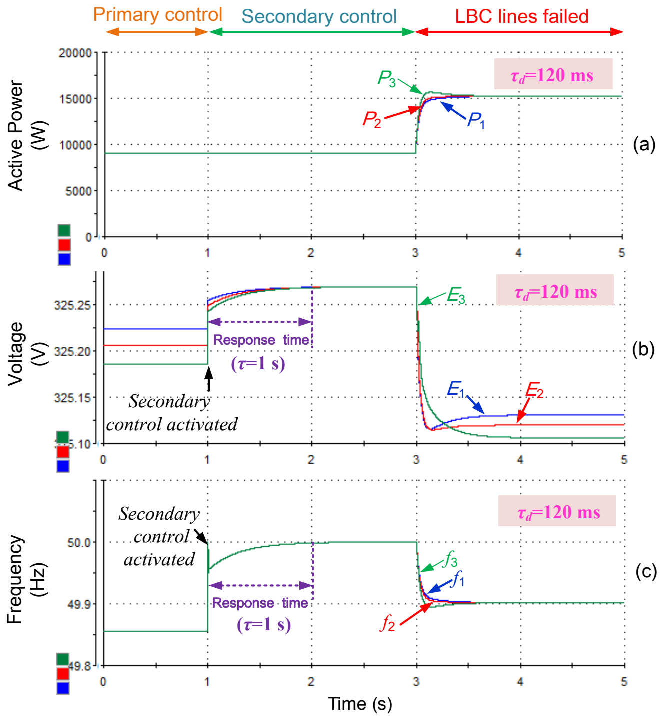

Fig. 9. Dynamic response of the islanded microgrid for the secondary control considering LBC delay. a) active power of each DG unit. b) output voltage of each DG unit. c) frequency of the microgrid.

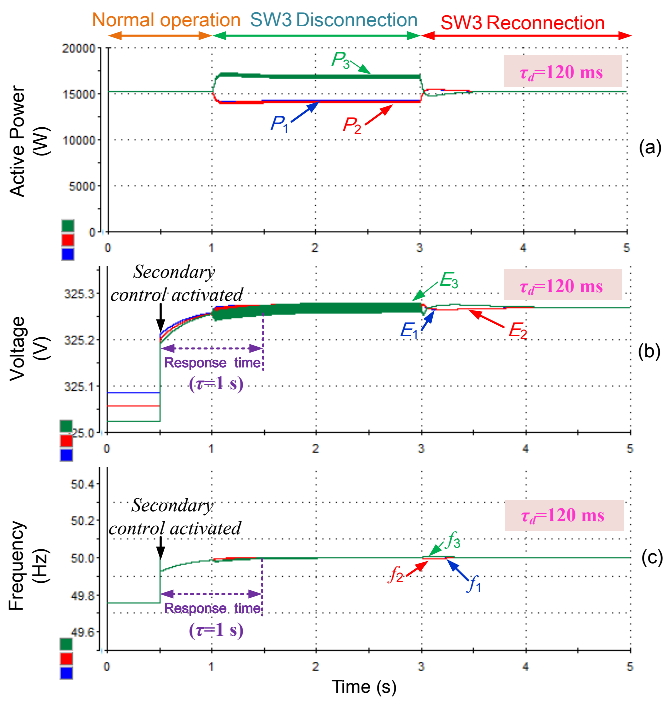

Fig.10. Dynamic response of the islanded microgrid for the secondary control considering feeder disturbances and LBC delay. a) active power of each DG unit. b) output voltage of each DG unit. c) frequency of the microgrid.

Fig. 12 shows the evaluation of dynamic stability of the islanded microgrid system under disturbance of feeders. In this scenario, the SW3 is disconnected at t=1s and reconnected at t=3s. It can be observed that the frequency and voltage can be recovered to the rated values within 1.25s. However, the voltage and frequency differences of the DG_2 reach to 0.72V and 0.57 Hz, respectively, which are even larger than the deviations caused by the droop control. Therefore, the dynamic stability of the microgrid needs to be further improved, when simultaneously restoring the frequency and voltage amplitude while sharing active power.

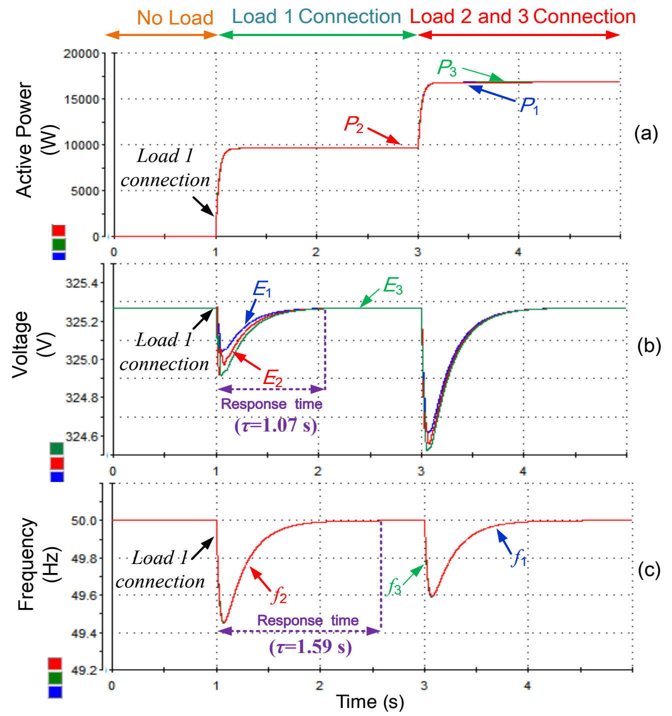

Fig. 11. Dynamic response of the islanded microgrid for the washout filter power sharing strategy under load disturbance conditions. a) active power of each DG unit. b) output voltage of each DG unit. c) frequency of the microgrid.

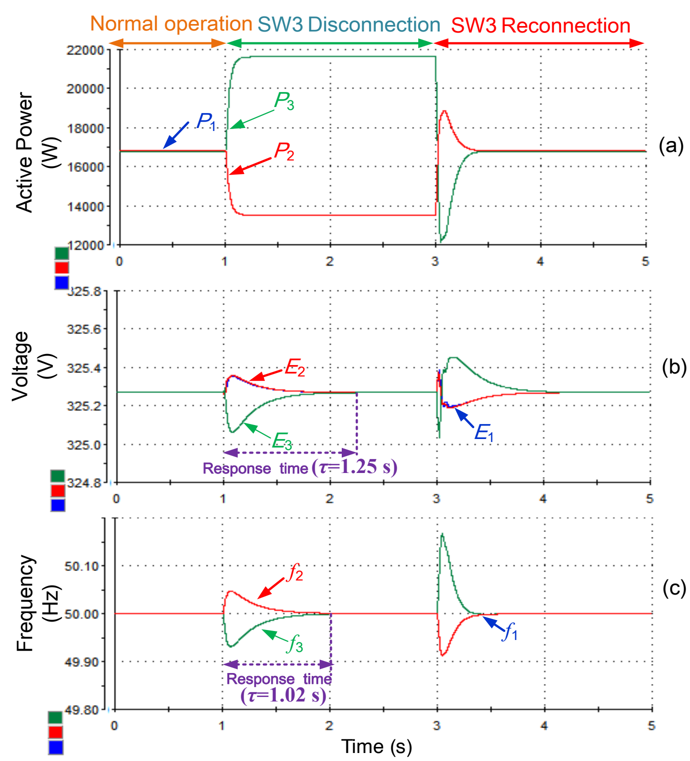

Fig. 12. Dynamic response of the islanded microgrid for the washout filter-based control under feeder disturbance conditions. a) active power of each DG unit. b) output voltage of each DG unit. c) frequency of the microgrid.

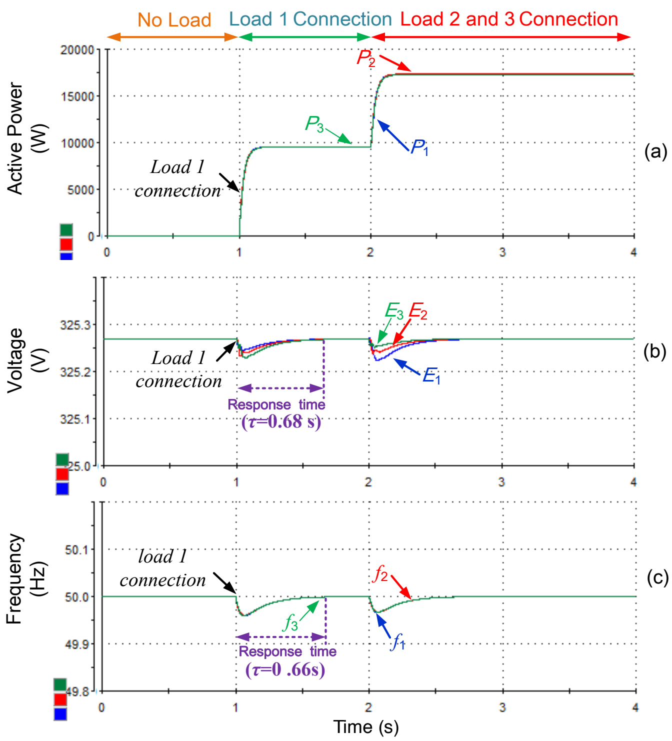

Fig. 13. Dynamic response of the islanded microgrid for the generalized washout filter-based control under load disturbance conditions. a) active power of each DG unit. b) output voltage of each DG unit. c) frequency of the microgrid.

D. Performance of the Generalized Washout Filter-based Control Strategy

When the generalized washout filter-based control scheme is activated for each DG unit, the precise active power sharing can

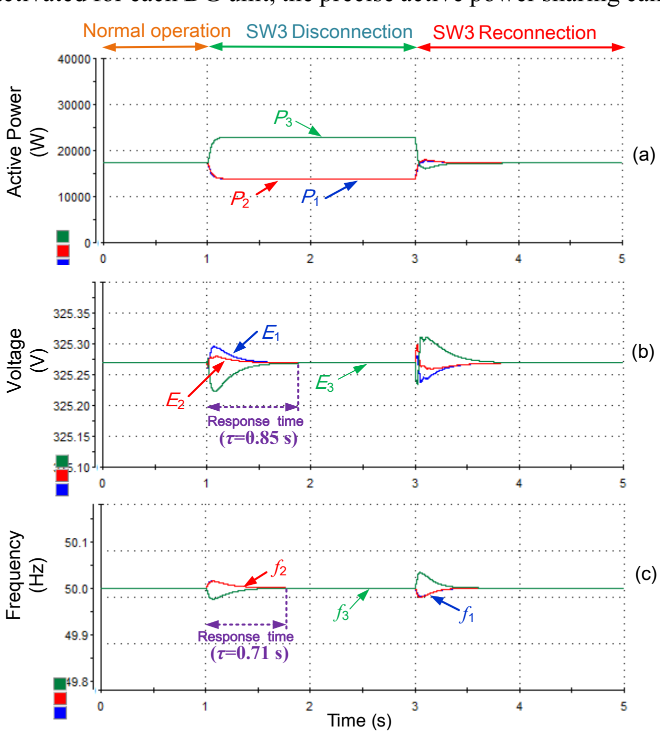

Fig. 14. Dynamic response of the islanded microgrid for the generalized washout filter-based control under feeder disturbance conditions. a) active power of each DG unit. b) output voltage of each DG unit. c) frequency of the microgrid.

be achieved in an islanded microgrid, as shown in Fig. 13(a). Moreover, the effect of unequal load impedances is considered, where inductance and resistance of load 1 are changed to 800 mH and 7 Ω, respectively. The load 1 is connected at t=1s and the rest of loads are connected to the microgrid at t=2s. Compared with the conventional droop control, the dynamic stability of the active power is significantly enhanced in Fig. 13(a). The same as the secondary control, frequency and voltage amplitude can be restored to the rated values in a short time (less than 0.68s). Moreover, compared with the washout filter-based and secondary control methods, there is only a small fluctuation in frequency and voltage amplitude less than 0.8% and 0.012%, respectively, with the disturbance of load impedance as shown in Fig. 11.

The effects of feeder and DG disturbances are shown in Fig. 14, where the SW3 is disconnected at t=1s and reconnected at t=3s. Moreover, unequal load impedances, where inductance and resistance of load 1 are changed to 800 mH and 7 Ω, respectively, are also considered in this scenario. It can be seen that the performance of the active power sharing, frequency and voltage regulation of the MG system can be ensured, and the difference in the transient behavior is negligible in comparison to the cases in the conventional droop control depicted in Fig. 8 and secondary control shown in Fig. 10. In addition, compared with the washout filter-based and secondary control methods, the maximum fluctuation of frequency and voltage amplitude less than 0.5% and 0.015%, respectively, with the disturbance of load impedance as shown in Fig. 14.

Note that no communication line is needed in the generalized washout filter-based control scheme, which is immune to the communication delay and data drop-out. Although both the washout filter-based control and secondary control can restore the frequency and voltage amplitude to the rated values when sharing the active powers, the generalized washout filter-based power sharing strategy is more robust to the LBC delay, the load/feeder/DG disturbances, and parameter uncertainties. Moreover, the dynamic stability is improved and the fluctuation of frequency and voltage amplitude are decreased significantly, compared with the washout filter-based control method.

V. Experimental Results

To evaluate the effectiveness of the generalized washout filter-based power sharing strategy, the experiments on a down-scaled parallel-connected three-phase inverters-based islanded microgrid was built, as shown in Fig. 15. In addition, the dc-link voltages for each inverter is set as 15V, with 10Ω load connected through LCL filters, where L_{f1}=L_{f2}=4 mH and L_{c1}=L_{c2}=1.35 mH, and the capacitor C_{f1}=C_{f2}=2.5 μF. The experimental setup is controlled by a TMS320F28335 digital signal processor (DSP), and other controller parameters of the islanded MG system are consistent with the theoretical analysis.

Fig.16 shows the experimental results under steady state operation of the generalized washout filter-based control scheme. As shown in Fig.16, output currents of DG_1 and DG_2 in phase 'a' are represented by i_{o1a} and i_{o2a}, respectively, and the load current and voltage in phase 'a' are represented by i_{loada}, v_{loada}, respectively. Initially, the DG units are disconnected to the microgrid and currents and voltage are equal to zero. When

DG units are abruptly connected to the system, the occurrence of current overshoots can be prevented by the effective voltage and current controllers and power sharing strategy. Moreover, in the steady-state conditions, experimental results indicate that output currents are in phase with the output voltages of the two inverters, and both parallel inverters share current equally. This suggests that the active power sharing is realized by generalized washout filter-based control strategy.

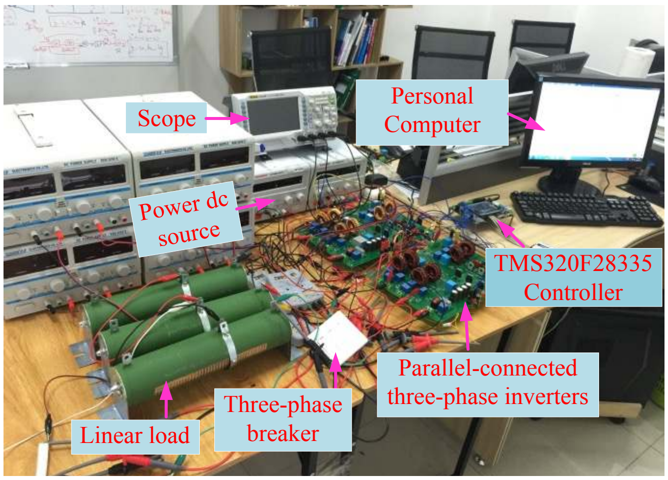

Fig. 15. Experimental setup for the down-scaled prototype AC microgrid.

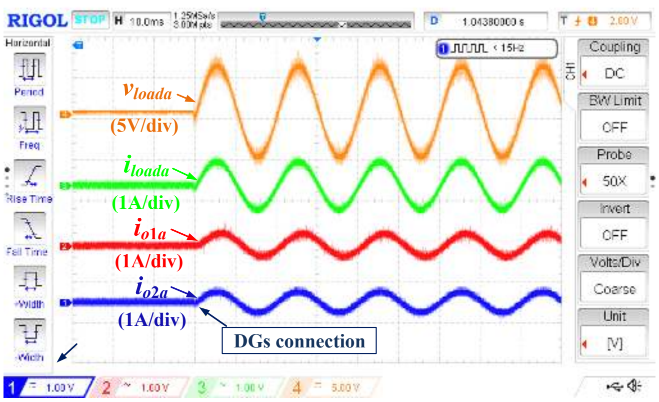

Fig. 16. Experimental waveforms of output currents of inverters, and output voltage and current of loads when DG units are connected to the microgrid.

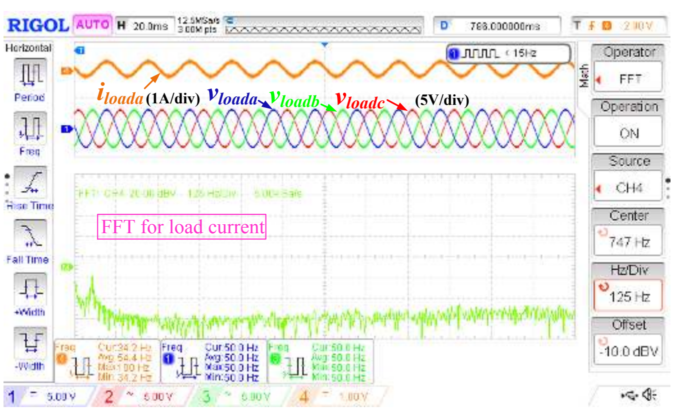

Fig. 17. Experimental waveforms of voltage and current of loads, and the FFT-curve of the A-phase load current in islanded microgrid.

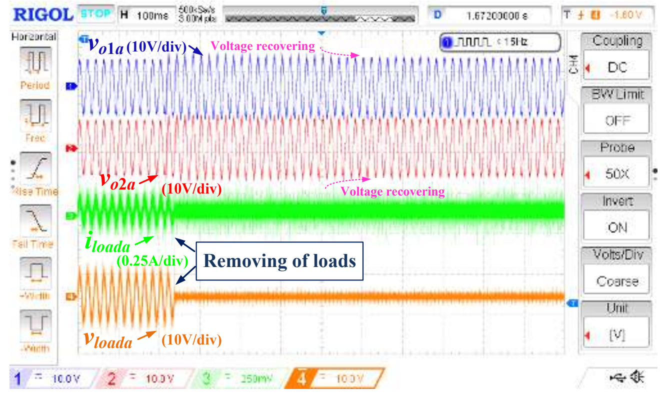

Fig. 18. Experimental waveforms of output voltages of inverters, and output voltage and current of loads when loads are disconnected to the microgrid.

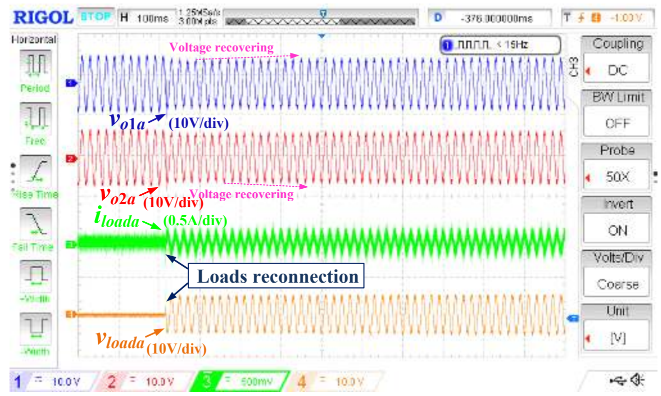

Fig. 19. Experimental waveforms of output voltages of inverters, and output voltage and current of loads when loads are reconnected to the microgrid.

The load voltage THD with the generalized washout filter-based control is less than 5%, which is shown in Fig.17. The negligible output harmonic contents of voltage further validate the effective performance of the current controllers and power sharing strategy.

Fig.18 and 19 show the steady-state and transient response of the generalized washout filter-based control scheme under the disturbance of loads. As shown in Fig.18, the voltage deviations are inevitable when the loads are disconnected to the microgrid system. However, the voltage can be restored to the rated values in a short time. Moreover, as depicted in Fig.19, the generalized washout filter-based control strategy can also eliminate the steady-state voltage deviations when the loads are reconnected. To conclude, the experimental results of the dynamic response of the voltage and current further verifies the effectiveness of the generalized washout filter-based control method.

VI. Future Research Trends

In a modern smart grid, multiple microgrids clusters are required to further improve the reliability, economic benefits, and environmental friendliness of the system. Additionally, in the case of connecting the MG to the other MGs, the tertiary control strategies, the consensus-based distributed control algorithms, multi-agent system control, etc., are popular to be employed to control the power/current flow between them, fulfil the power quality requirements and enhance the robust and dynamic stability of MGs [28-32], [53-57]. However, the communication links are inevitable to be utilized to exchange information among multiple DG units and microgrids.

To overcome the shortcomings of the hierarchical controlled microgrid under communication delay, the promising future study directions are outlined as follows.

A. The Tertiary Control for Microgrids

Modern MGs can switch between the grid-connected and islanded modes, and the tertiary control is needed to ensure to inject the dispatched power to the main grid, as well as to deal with economic dispatching, operation scheduling, and power flow regulation between the MG and grid [53], [54].

Note that the high band-width communication (HBC) links are required in the hierarchical control strategy, which decrease the reliability, robustness and dynamic stability of the system. Therefore, an equivalent tertiary control could be used to coordinate multiple microgrids, where the communication links can be reduced or eliminated, hence significantly reduce the cost and enhance the reliability and robustness of the system.

B. The Consensus-based Control Strategy for Microgrids

In consideration of the multiple DG units in microgrids, the conventional centralized control scheme faces new challenges, such as the requirement for more sophisticated control center, increased computational burden, and complex communication configuration, grid scalability, and etc. [28], [55]. Recently, the consensus-based distributed control scheme for networked systems has been introduced to address these challenges [28], [55], [56]. The general purpose of consensus algorithms is to allow a set of agents to reach an agreement on a quantity of interest by exchanging information through communication networks [56]. These kinds of agents are only required to communicate with their neighbors. As the foundation of the distributed control scheme, the communication network may not always be fully reliable, which could lead to serious security problems. Therefore, it's valuable to study the equivalent consensus algorithm to enhance the reliability and robustness of the hierarchical controlled microgrids under LBC delays.

C. The Multi-Agent System in Microgrids

Multi-agent system (MAS) is popularly used to exchange information among multiple agents by communication with their corresponding neighbors through some computer network infrastructure [32], [55]. Furthermore, the global information discovery algorithm is independent of the system configuration, thus it can be applied to the microgrid system of any structures, such as radial, mesh and mixed topologies [57]. Therefore, the microgrid can be coordinated in a decentralized way, and the effect on communication delay can be decreased significantly, when the proposed method is extended to analyze the possible equivalence among agents in the top and bottom layers.

VII. CONCLUSION

This paper reveals that there is an equivalence between a washout filter-based strategy and secondary control, and the physical meaning of parameters of secondary controllers is discussed, emphasizing that the proportional and integral coefficients of the secondary controller are used to form a band-pass filter. In addition, a generalized washout filter-based power sharing strategy has been obtained to significantly improve the dynamic stability of the system, which can be considered as an enhanced washout filter-based method. Compared to the secondary control, the generalized washout-filter based control method can eliminate the steady state errors in the output voltage amplitude and frequency due to the droop control without using LBC links. Compared to the existing washout filter-based control method, the generalized washout filter-based control shows the benefits of enhanced dynamic response under load and feeder disturbances and reduced over-shoots in the output voltages under dynamic disturbances.

A complete small-signal model of the generalized washout-filter control scheme is proposed in this paper, which can be applied to design of control parameters of the equivalent control model and analyze the stability of the MG. The hardware-in-the-loop (HIL) results of the conventional droop control, secondary control with LBC delay, washout filter-based method and generalized washout filter-based power sharing scheme are given under unequal feeder impedances and load/DG disturbance conditions to show the effectiveness of the theoretical findings.

In addition, the experimental results further validate that the proposed approach are capable to restore the voltages to the rated values without any LBC line and extra control loop, which are more robust to the low bandwidth communication delay and load/DG disturbance. Finally, the promising directions for future research to improve the hierarchical control strategies considering communication delay are summarized.

APPENDIX A

The matrix $\mathbf{T_{BPF}}$ of power stage is derived as (A.1), and the elements in matrix $\mathbf{T_{BPF}}$ are depicted as (A.2) and (A.3):

$$\mathbf{T_{BPF}} = \begin{bmatrix} -\omega_h & k_2\omega_c & 0 & 0 & 0 \\ 0 & -\omega_c & 0 & 0 & 0 \\ 0 & 0 & -\omega_c & 0 & 0 \\ -v_q & 0 & k_3 v_d & -\dfrac{\omega_h v_d^2}{v_d^2+v_q^2} & -\dfrac{\omega_h v_d v_q}{v_d^2+v_q^2} \\ v_d & 0 & k_3 v_q & -\dfrac{\omega_h v_d v_q}{v_d^2+v_q^2} & -\dfrac{\omega_h v_q^2}{v_d^2+v_q^2} \end{bmatrix}_{5\times5} \quad (A.1)$$

$$k_1 = \frac{n_q}{1+k_{pE}}, k_2 = \frac{m_p}{1+k_{p\omega}},\ k_3 = \frac{k_1\omega_c\sqrt{v_d^2+v_q^2}}{v_d^2+v_q^2} \quad (A.2)$$

$$\omega_{hE} = \frac{k_{iE}}{1+k_{pE}},\ \omega_{h\omega} = \frac{k_{i\omega}}{1+k_{p\omega}} \quad (A.3)$$

The matrices $\mathbf{C_V}$, $\mathbf{D_{V1}}$, $\mathbf{D_{V2}}$ and $\mathbf{B_{V2}}$ in the inner voltage controller are derived as:

$$\mathbf{C_V} = \begin{bmatrix} k_{iv} & 0 \\ 0 & k_{iv} \end{bmatrix}_{2\times2},\ \mathbf{D_{V2}} = \begin{bmatrix} 0 & 0 & -k_{pv} & -\omega^* C_f & F & 0 \\ 0 & 0 & \omega^* C_f & -k_{pv} & 0 & F \end{bmatrix}_{2\times6} \quad (A.4)$$

$$\mathbf{D_{V1}} = \begin{bmatrix} k_{pv} & 0 \\ 0 & k_{pv} \end{bmatrix}_{2\times2},\ \mathbf{B_{V2}} = \begin{bmatrix} 0 & 0 & -1 & 0 & 0 & 0 \\ 0 & 0 & 0 & -1 & 0 & 0 \end{bmatrix}_{2\times6} \quad (A.5)$$

The matrices $\mathbf{C_C}$, $\mathbf{D_{C1}}$, $\mathbf{D_{C2}}$ and $\mathbf{B_{C2}}$ in the inner current controller are derived as:

$$\mathbf{C_C} = \begin{bmatrix} k_{ic} & 0 \\ 0 & k_{ic} \end{bmatrix}_{2\times2},\ \mathbf{D_{C2}} = \begin{bmatrix} -k_{pc} & -\omega^* L_f & 0 & 0 & 0 & 0 \\ \omega^* L_f & -k_{pc} & 0 & 0 & 0 & 0 \end{bmatrix}_{2\times6} \quad (A.6)$$

$$\mathbf{D_{C1}} = \begin{bmatrix} k_{pc} & 0 \\ 0 & k_{pc} \end{bmatrix}_{2\times2}, \ \mathbf{B_{C2}} = \begin{bmatrix} -1 & 0 & 0 & 0 & 0 & 0 \\ 0 & -1 & 0 & 0 & 0 & 0 \end{bmatrix}_{2\times6} \quad (A.7)$$

The matrices $\mathbf{A_{LCL}}$, $\mathbf{B_{LCL1}}$, $\mathbf{B_{LCL2}}$ and $\mathbf{B_{LCL3}}$ in (20) are derived as (A.8) and (A.9).

$$\mathbf{A_{LCL}} = \begin{bmatrix} -\frac{r_{L_f}}{L_f} & \omega^* & -\frac{1}{L_f} & 0 & 0 & 0 \\ -\omega^* & -\frac{r_{L_f}}{L_f} & 0 & -\frac{1}{L_f} & 0 & 0 \\ \frac{1}{C_f} & 0 & 0 & \omega^* & -\frac{1}{C_f} & 0 \\ 0 & \frac{1}{C_f} & -\omega^* & 0 & 0 & -\frac{1}{C_f} \\ 0 & 0 & \frac{1}{L_c} & 0 & -\frac{r_{L_c}}{L_c} & \omega^* \\ 0 & 0 & 0 & \frac{1}{L_c} & -\omega^* & -\frac{r_{L_c}}{L_c} \end{bmatrix}_{6\times6} \quad (A.8)$$

$$\mathbf{B_{LCL1}} = \begin{bmatrix} \frac{1}{L_f} & 0 \\ 0 & \frac{1}{L_f} \\ 0 & 0 \\ 0 & 0 \\ 0 & 0 \\ 0 & 0 \end{bmatrix}_{6\times2}, \mathbf{B_{LCL2}} = \begin{bmatrix} 0 & 0 \\ 0 & 0 \\ 0 & 0 \\ 0 & 0 \\ -\frac{1}{L_c} & 0 \\ 0 & -\frac{1}{L_c} \end{bmatrix}_{6\times2} \quad \mathbf{B_{LCL3}} = \begin{bmatrix} I_{lq} \\ -I_{ld} \\ V_{oq} \\ -V_{od} \\ I_{oq} \\ -I_{od} \end{bmatrix}_{6\times1} \quad (A.9)$$

REFERENCES

[1] J. Rocabert, A. Luna, F. Blaabjerg and P. Rodrıguez, "Control of power converters in AC microgrids," *IEEE Trans. Power Electron*., vol. 27, no. 11, pp. 4734-4749, Nov. 2012.

[2] S. Khan, W. Gawlik and P. Palensky, "Reserve capability assessment considering correlated uncertainty in microgrid," *IEEE Trans. Sustain. Energy*., vol. 7, no. 2, pp. 637-646, Apr. 2016.

[3] P. Li, D. X, Z. Y. Zhou, W. J. Lee and B. Zhao, "Stochastic optimal operation of microgrid based on chaotic binary particle swarm optimization," *IEEE Trans. Smart Grid*., vol. 7, no. 1, pp. 66-73, Jan. 2016.

[4] Z. L. Zhao, P. Yang, J. M. Guerrero, Z. R. Xu and T. C. Green, "Multiple-time-scales hierarchical frequency stability control strategy of medium-voltage isolated microgrid," *IEEE Trans. Power Electron*., vol. 31, no. 8, pp. 5974-5991, Aug. 2016.

[5] W. Pei, Y. Du, W. Deng, K. Sheng, H. Xiao and H. Qu, "Optimal bidding strategy and intramarket mechanism of microgrid aggregator in real-time balancing market," *IEEE Trans. Ind. Informat.,* vol. 12, no. 2, pp. 587-596, Apr. 2016.

[6] Y. Lan, X. H. Guan and J. Wu, "Rollout strategies for real-time multi-energy scheduling in microgrid with storage system," *IET Gener. Transm. Distrib*., Vol. 10, no. 3, pp. 688–696, 2016.

[7] L. Wang, D. L. Zhang, Y. Wang, B. Wu and H. S. Athab, "Power and voltage balance control of a novel three-phase solid-state transformer using multilevel cascaded H-bridge inverters for microgrid applications," *IEEE Trans. Power Electron*., vol. 31, no. 4, pp. 3289-3310, Apr. 2016.

[8] Z. Y. Yang, R. Wu, J. F. Yang, K. Y. Long and P. C. You, "Economical operation of microgrid with various devices via distributed optimization," *IEEE Trans. Smart Grid*., vol. 7, no. 2, pp. 857-867, Mar. 2016.

[9] S. X. Wang, X. Y. Zhang, L. J. Ge and L. Wu, "2-D wind speed statistical model for reliability assessment of microgrid," *IEEE Trans. Sustain. Energy*., vol. 7, no. 3, pp. 1159-1169, Jul. 2016.

[10] Y. X. Zhu, F. Zhuo, F. Wang, B. Q. Liu, R. F. Gou and Y. J. Zhao, "A virtual impedance optimization method for reactive power sharing in networked microgrid," *IEEE Trans. Power Electron*., vol. 31, no. 4, pp. 2890-2904, Apr. 2016.

[11] G. D. Liu, Y. Xu and K. Tomsovic, "Bidding strategy for microgrid in day-ahead market based on hybrid stochastic/robust optimization," *IEEE Trans. Smart Grid*., vol. 7, no. 1, pp. 227-237, Jan. 2016.

[12] A. Mondal, M. S. Illindala, A. S. Khalsa, D. A. Klapp and J. H. Eto, "Design and Operation of Smart Loads to Prevent Stalling in a Microgrid," *IEEE Trans. Ind. Appl.,* vol. 52, no. 2, pp. 1184-1192, Mar/Apr. 2016.

[13] K. Yu, Q. Ai, S. Y. Wang, J. M. Ni and T. G. Lv, "Microgrid system based on small-signal dynamic model," *IEEE Trans. Smart Grid*., vol. 7, no. 2, pp. 695-705, Mar. 2016.

[14] Y. A. R. I. Mohamed and A. A. Radwan, "Hierarchical control system for robust microgrid operation and seamless mode transfer in active distribution systems," *IEEE Trans. Smart Grid*., vol. 6, no. 4, pp. 352–362, Jun. 2011.

[15] A. Kahrobaeian and Y. A. R. I. Mohamed, "Networked-based hybrid distributed power sharing and control for islanded microgrid systems" *IEEE Trans. Power Electron*., vol. 30, no. 2, pp. 603–617, Feb. 2015.

[16] X. Q. Lu, X. H. Yu, J. G. Lai, Y. N. Wang and J. M. Guerrero, "A novel distributed secondary coordination control approach for islanded microgrids," *IEEE Trans. Smart Grid*., to be published, doi: 10.1109/TSG.2016.2618120

[17] I. U. Nutkani, P. C. Loh, P. Wang and F. Blaabjerg, "Linear decentralized power sharing schemes for economic operation of AC microgrids," *IEEE Trans. Ind. Electron*., vol. 63, no. 1, pp. 225–234, Jan. 2016.

[18] X. S. Tang, X. Hu, N. N. Li, W. Deng and G. W. Zhang, "A novel frequency and voltage control method for islanded microgrid based on multi energy storages," *IEEE Trans. Smart Grid*., vol. 7, no. 1, pp. 410-419, Jan. 2016.

[19] H. G. Xiao, A. Luo, Z. K. Shuai, G. B. Jin and Y. Huang, "An improved control method for multiple bidirectional power converters in hybrid AC/DC microgrid," *IEEE Trans. Smart Grid*., vol. 7, no. 1, pp. 340-347, Jan. 2016.

[20] T. Wu, Z. Liu, J. J Liu, S. Wang and Z. Y. You, "A unified virtual power decoupling method for droop-controlled parallel inverters in microgrids," *IEEE Trans. Power Electron*., vol. 31, no. 8, pp. 5587-5603, Aug. 2016.

[21] Ahmadi, H. Bevrani, S. Shokoohi amd E. Hasanii, "An improved droop control for simultaneous voltage and frequency regulation in an AC microgrid using fuzzy logic," in *proc. 23rd Iranian Conf. on Electrical Engineering (ICEE)*, pp. 1486-1491, 2015.

[22] H. C. Chiang, K. K. Jen, G. H. You, "Improved droop control method with precise current sharing and voltage regulation," *IET Gener. Transm. Distrib*., Vol. 9, no. 4, pp. 789–800, 2016.

[23] N. L. D´ıaz, D. Wu, T. Dragiˇcevi´c, J. C. V´asquez and J. M. Guerrero, "Fuzzy droop control loops adjustment for stored energy balance in distributed energy storage system," in *proc. 9th International Power Electronics and Motion Control Conf. (ECCE)*, pp. 1-5, Jun. 2015.

[24] J. M. Guerrero, J. Matas, V. L. De, M. Castilla, and J. Miret, "Wireless control strategy for parallel operation of distributed-generation inverters," *IEEE Trans. Ind. Electron*., vol. 53, no. 5, pp. 1461–1470, Oct. 2006.

[25] J. M. Guerrero, J. C. Vasquez, J. Matas, M. Castilla, and V. L. De, "Control strategy for flexible microgrid based on parallel line-interactive UPS systems," *IEEE Trans. Ind. Electron*., vol. 56, no. 3, pp. 726–736, Mar. 2009.

[26] J. M. Guerrero, J. C. Vasquez, J. Matas, L. G. D. Vicuna and M. Castilla, "Hierarchical control of droop-controlled AC and DC microgrids-general approach toward standardization," *IEEE Trans. Ind. Electron*., vol. 58, no. 1, pp. 158-172, Jan. 2011.

[27] Q. Shafiee, J. M. Guerrero and J. C. Vasquez, "Distributed secondary control for islanded microgrids—a novel approach," *IEEE Trans. Power Electron*., vol. 29, no. 2, pp. 1018-1031, Feb. 2014.

[28] D. W. He, D. Shi, and R. Sharma, "Consensus-based distributed cooperative control for microgrid voltage regulation and reactive power sharing," in *proc. IEEE PES Innovative Smart Grid Technologies Conf. Europe (ISGT-Europe)*, 2014, pp. 1-6.

[29] A. Bidram, A. Davoudi and F. L. Lewis, "Two-layer distributed cooperative control of multi-inverter microgrids," in *proc. IEEE 29th. Applied Power Electronics Conference and Exposition Annu. Conf. (APEC)*, 2014, pp. 2364-2371.

[30] J. W. S. Porco, Q. Shafiee, F. Dorfler, J. C. Vasquez, J. M. Guerrero and F. Bullo, "Secondary frequency and voltage control of islanded microgrids via distributed averaging," *IEEE Trans. Ind. Electron*., vol. 62, no. 11, pp. 7025-7038, Nov. 2015.

[31] Y. Zhang, R. Wang, T. Zhang, Y. J. Liu, B. Guo, "Model predictive control-based operation management for a residential microgrid with considering forecast uncertainties and demand response strategies," *IET Gener. Transm. Distrib*., Vol. 10, no. 10, pp. 2367-2378, 2016.

[32] Q. Li, F. X. Chen, M. Chen, J. M. Guerrero and D. Abbott, "Agent-based decentralized control method for islanded microgrids," *IEEE Trans. Smart Grid*., vol. 7, no. 2, pp. 637-649, 2016.
[33] S. C. Liu, X. Y. Wang, and P. X. P. Liu, "Impact of communication delays on secondary frequency control in an islanded microgrid," *IEEE Trans. Ind. Electron*., vol. 62, no. 4, pp. 2021-2031, Apr. 2015.
[34] C. Ahumada, R. Cardenas, D. Saez and J. M. Guerrero, "Secondary control strategies for frequency restoration in islanded microgrids with consideration of communication delays," *IEEE Trans. Smart Grid*., vol. 7, no. 3, pp. 1430-1441, 2016.
[35] M. Yazdanian, and A. M. Sani, "Washout Filter-Based Power Sharing," *IEEE Trans. Smart Grid*., vol. 7, no. 2, pp. 967-968, Mar. 2016.
[36] J. M. Guerrero, M. Chandorkar, T. Lee and P. C. Loh, "Advanced control architectures for intelligent microgrids-part I: decentralized and hierarchical control," *IEEE Trans. Ind. Electron*., vol. 60, no. 4, pp. 1254-1262, Apr. 2013.
[37] O. Palizban, and K. kaohaniemi, "Hierarchical control structure in microgrids with distributed generation: island and grid-connected mode," *Renew. Sustain. Energy Rev*., vol. 44, pp. 797-813, Apr. 2015.
[38] Q. Shafiee, C. Stefanovic, T. Dragicevic, P. Popovski, J. C. Vasquez and J. M. Guerrero, "Robust networked control scheme for distributed secondary control of islanded microgrids," *IEEE Trans. Ind. Electron*., vol. 61, no. 10, pp. 5363–5374, Oct. 2014.
[39] P. B. Wang, X. N. Lu, X. Yang, W. Wang and D. G. Xu, "An improved distributed secondary control method for DC microgrids with enhanced dynamic current sharing performance," *IEEE Trans. Power Electron*., vol. 31, no. 9, pp. 6658-6673, Sep. 2015.
[40] H. G. Zhang, S. Kim, Q.Y. Sunand J. G. Zhou, "Distributed adaptive virtual impedance controlfor accurate reactive power sharing basedon consensus control in microgrids," *IEEE Trans. Smart Grid*., to be published, doi: 10.1109/TSG.2015.2506760.
[41] S. Liu, Y. Zhang, L. Li, J. Hu, Y. F. Zhou, W. Zhao and R. M. Xu, "220GHz band-pass filter based on circular resonance cavities with low loss," in *proc. 45th Proceedings of the European Microwave Conf. (EuMC)*, 1077-1079, 2015.
[42] A. Q. Liu, A. B. Yu and Q. X. Zhang, "Broad-band band-pass and band-stop filters with Sharp Cut-off frequencies based on series CPW stubs," in *proc. IEEE International MTT-S Microwave Symposium Digest*, pp. 353-356, 2006.
[43] K. Yu, Q. Ai , S. Y. Wang, J. M. Ni, and T. G. Lv, "Analysis and optimization of droop controller for microgrid system based on small-signal dynamic model," *IEEE Trans. Smart Grid*., vol. 7, no. 2, pp. 695-705, Mar. 2016.
[44] W. Cao, H. Su, J. L. Cao, J. Sun and D. P. Yang, "Improved droop control method in microgrid and its small signal stability analysis," in *proc. 3rd International Conf. on Renew. Energy Research and Appl.*, pp. 197-202, 2014.
[45] H. T. Shi, F. Zhuo, L. X. Hou, X. L. Yue, D. Zhang, "Small-signal stability analysis of a microgrid operating in droop control mode," in *proc. IEEE Asia Power Electronics and Motion Control Conf. (ECCE)*, 2013.
[46] J. Ma, X. Wang and X. B. Lan, "Small-signal Stability Analysis of Microgrid based on perturbation theory," in *proc. Asia-Pacific Power and Energy Engineering Conf.*, 2012.
[47] N. Pogaku; M. Prodanovic; T. C. Green, "Inverter-based microgrids: Small-signal modelling and testing," in *proc. 3rd International Power electronics, machines and drives (PEMD) Conf.*, 2006.
[48] Y. A. R. I. Mohamed and E. F. E. Saadany, "Adaptive decentralized droop controller to preserve power sharing stability of paralleled inverters in distributed generation microgrids," *IEEE Trans. Power Electron*., vol. 23, no. 6, pp. 2806-2816, Nov. 2008.
[49] D. Jie, Z. C. Jiang, M. X. Mai, G. Z. Nan, K. Z. Zhong, "Modeling and stability analysis of autonomous microgrid composed of inverters based on improved droop control," in *proc. 3rd International Power Electronics and Application Conf. and Exposition*, 2014.
[50] D. K. Dheer, N. Soni, S. Doolla, "Small signal stability in microgrids with high penetration of power electronics interfaced sources," in *proc. 40th IEEE. International Industrial Electronics Society Conf.(IECON)*, 2014.
[51] M. Rasheduzzaman, J. A. Mueller and J. W. Kimball, "An accurate small-signal model of inverter-dominated islanded microgrids using dq reference frame," *IEEE J. Emerg. Sel. Topics Power Electron*., vol. 2, no. 4, pp. 1070–1080, Dec. 2014.
[52] N. Pogaku, M. Prodanovic and T. C. Green, "Modeling, analysis and testing of autonomous operation of an inverter-based microgrid," *IEEE Trans. Power Electron*., vol. 22, no. 2, pp. 613-625, Mar. 2007.
[53] D. E. Olivares, A. M. Sani, A. H. Etemadi, C. A. Cañizares, R. Iravani, M. Kazerani, A. H. Hajimiragha, Claudio. A. Canizares, R. Iravani, M. Kazerani, A. H. Hajimiragha, O. G. Bellmunt, M. Saeedifard, R. P. Behnke, G. A. J. Estévez and N. D. Hatziargyriou, "Trends in microgrid control," *IEEE Trans. Smart Grid*., vol. 5, no. 4, pp. 1905-1919, Jul. 2014.
[54] S. Moayedi and A. Davoudi, "Distributed tertiary control of DC microgrid clusters," *IEEE Trans. Power Electron*., vol. 31, no. 2, pp. 1717-1733, Feb. 2016.
[55] Y. L. Xu and Z. C. Li, "Distributed optimal resource management based on the consensus algorithm in a microgrid," *IEEE Trans. Ind. Electron.*, vol. 62, no. 4, pp. 2584-2592, Apr. 2015.
[56] L. X. Meng, T. Dragicevic, J. Pérez, J. C. Vasquez and J. M. Guerrero, Fellow, "Modeling and sensitivity study of consensus algorithm-based distributed hierarchical control for DC microgrids," *IEEE Trans. Smart Grid*., vol. 7, no. 3, pp. 1504-1515, May. 2016.
[57] T. Morstyn, B. Hredzak and V. G. Agelidis, "Decentralized reactive power sharing and frequency restoration in islanded microgrid,"*IEEE Trans. Power Syst*., vol. 31, no. 4, pp. 2974-2986, Jul. 2016.

Yang Han (S'08-M'10) received the B.S. degree in Electrical Engineering from University of Electronic Science and Technology of China (UESTC), Chengdu, China, in 2004, and received the Ph.D. in Electrical Engineering from Shanghai Jiaotong University (SJTU), Shanghai, China, in 2010. He joined the Department of Power Electronics, School of Mechatronics Engineering, University of Electronic Science and Technology of China (UESTC) in 2010, and has been promoted to an Associate Professor since 2013. From March 2014 to March 2015, he was a visiting scholar (guest postdoc) in the area of renewable energy and microgrids at the Department of Energy Technology, Aalborg University, Aalborg, Denmark. His research interests include AC/DC microgrids, grid-connected converters for renewable energy systems and DGs, phase-locked loop (PLL), power quality, multilevel converters, active power filters and static synchronous compensators (STATCOMs) for smart grid applications.

He has authored more than 20 SCIE-indexed journal papers and one book chapter in the area of power electronics, power quality conditioners, and smart grid. He has served as the Session Chair in "AC/DC, DC/AC Power Converter" session in the IPEMC 2016-ECCE Asia in Hefei, China. He has been awarded "2016 Baekhyun Award" for his contribution to the field of power electronics by the Korean Institute of Power Electronics (KIPE). He received the Best Paper Awards from 2013 Annual Conference of HVDC and Power Electronics Committee of Chinese Society of Electrical Engineers (CSEE) in Chongqing, China, and the 4th International Conference on Power Quality in 2008, in Yangzhou, China. He has seven issued and thirteen pending patents. Currently, he is the supervisor for nine master students, one of which has been nominated as provincial outstanding graduate student. He is an active reviewer for IEEE Transactions on Power Electronics, IEEE Transactions on Smart Grid, IEEE Transactions on Industrial Electronics, IEEE Transactions on Sustainable Energy and IEEE Transactions on Energy Conversion.

Hong Li received the B.S. degree in Electrical Engineering and Automation from University of Electronic Science and Technology of China (UESTC), Chengdu, China, in 2015. He is currently working towards the M.S. degree in Power Electronics and Electric Drives at UESTC, Chengdu, China. His current research interests include the optimization of ac microgrids, power management, hierarchical and cooperative control, and grid-integration of renewable energy resources.

Lin Xu received the Ph.D. degree in Electrical Engineering from Shanghai JiaoTong University (SJTU), Shanghai, China, in 2011. Currently, she is a Senior Engineering at Sichuan Electric Power Research Institute, State Grid Sichuan Electric Power Company, Chengdu, China. She has co-authored more than 20 journal and conference papers in the area of power electronics and power systems. Her research interests include power quality, power system analysis and real-time digital simulator (RTDS), flexible Ac transmission systems (FACTS), such as STATCOMs and power quality conditioners (DVRs, APFs). She is an active

reviewer for IEEE Transactions on Industrial Electronics, IEEE Transactions on Power Electronics, Electric Power Components and Systems, etc.

Xin Zhao received the B.S. and M.S. degree in Power Electronics & Electrical Drives from Northwestern Polytechnical University, Xi'an, China, in 2010 and 2013, respectively. He is currently working toward the Ph.D. degree at Department of Energy Technology, Aalborg University, Denmark. His research interests include control of power converters, power quality and microgrids.

Josep M. Guerrero (S'01-M'04-SM'08-FM'15) received the B.S. degree in telecommunications engineering, the M.S. degree in electronics engineering, and the Ph.D. degree in power electronics from the Technical University of Catalonia, Barcelona, in 1997, 2000 and 2003, respectively. Since 2011, he has been a Full Professor with the Department of Energy Technology, Aalborg University, Denmark, where he is responsible for the Microgrid Research Program (www.microgrids.et.aau.dk). From 2012 he is a guest Professor at the Chinese Academy of Science and the Nanjing University of Aeronautics and Astronautics; from 2014 he is chair Professor in Shandong University; from 2015 he is a distinguished guest Professor in Hunan University; and from 2016 he is a visiting professor fellow at Aston University, UK, and a guest Professor at the Nanjing University of Posts and Telecommunications.
His research interests is oriented to different microgrid aspects, including power electronics, distributed energy-storage systems, hierarchical and cooperative control, energy management systems, smart metering and the internet of things for AC/DC microgrid clusters and islanded minigrids; recently specially focused on maritime microgrids for electrical ships, vessels, ferries and seaports. Prof. Guerrero is an Associate Editor for the IEEE TRANSACTIONS ON POWER ELECTRONICS, the IEEE TRANSACTIONS ON INDUSTRIAL ELECTRONICS, and the IEEE Industrial Electronics Magazine, and an Editor for the IEEE TRANSACTIONS on SMART GRID and IEEE TRANSACTIONS on ENERGY CONVERSION. He has been Guest Editor of the IEEE TRANSACTIONS ON POWER ELECTRONICS Special Issues: Power Electronics for Wind Energy Conversion and Power Electronics for Microgrids; the IEEE TRANSACTIONS ON INDUSTRIAL ELECTRONICS Special Sections: Uninterruptible Power Supplies systems, Renewable Energy Systems, Distributed Generation and Microgrids, and Industrial Applications and Implementation Issues of the Kalman Filter; the IEEE TRANSACTIONS on SMART GRID Special Issues: Smart DC Distribution Systems and Power Quality in Smart Grids; the IEEE TRANSACTIONS on ENERGY CONVERSION Special Issue on Energy Conversion in Next-generation Electric Ships. He was the chair of the Renewable Energy Systems Technical Committee of the IEEE Industrial Electronics Society. He received the best paper award of the IEEE Transactions on Energy Conversion for the period 2014-2015, and the best paper prize of IEEE-PES in 2015. As well, he received the best paper award of the Journal of Power Electronics in 2016. In 2014, 2015, and 2016 he was awarded by Thomson Reuters as Highly Cited Researcher, and in 2015 he was elevated as IEEE Fellow for his contributions on "distributed power systems and microgrids."